Supporting Information

Structure-Property Relationships Based on Hammett Constants in Cyclometalated Iridium(III) Complexes: Application to the Design of a Fluorine-free FIrPic-like Emitter

Julien E. Frey,[a] Basile F. E. Curchod,[b] Rosario Scopelliti,[a] Ivano Tavernelli,[b] Ursula Rothlisberger,[b] Mohammad K. Nazeeruddin,[a] Etienne Baranoff[,c]*

[a] Laboratory of Photonics and Interfaces, Institute of Chemical Sciences and Engineering, École Polytechnique Fédérale de Lausanne, CH-1015 Lausanne, Switzerland

[b] Laboratory of Computational Chemistry and Biochemistry, Institute of Chemical Sciences and Engineering, École Polytechnique Fédérale de Lausanne, CH-1015 Lausanne, Switzerland

[c] School of Chemistry, University of Birmingham, Edgbaston, Birmingham B15 2TT, UK

E–mail: e.baranoff@bham.ac.uk

Scheme S1. Chemical structures of tris-homoleptic iridium complexes from ref. 1.

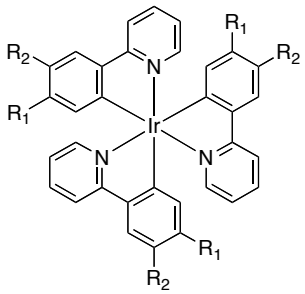

$\mathbf{R_1}$ = H, $\mathbf{R_2}$ = H : [Ir(ppy)$_3$]
$\mathbf{R_1}$ = Me, $\mathbf{R_2}$ = H : [Ir(4-Me-ppy)$_3$]
$\mathbf{R_1}$ = Pr, $\mathbf{R_2}$ = H : [Ir(4-Pr-ppy)$_3$]
$\mathbf{R_1}$ = tBu, $\mathbf{R_2}$ = H : [Ir(4-tBu-ppy)$_3$]
$\mathbf{R_1}$ = F, $\mathbf{R_2}$ = H : [Ir(4-F-ppy)$_3$]
$\mathbf{R_1}$ = CF_3, $\mathbf{R_2}$ = H : [Ir(4-CF_3-ppy)$_3$]
$\mathbf{R_1}$ = OMe, $\mathbf{R_2}$ = H : [Ir(4-OMe-ppy)$_3$]
$\mathbf{R_1}$ = H, $\mathbf{R_2}$ = OMe : [Ir(5-OMe-ppy)$_3$]

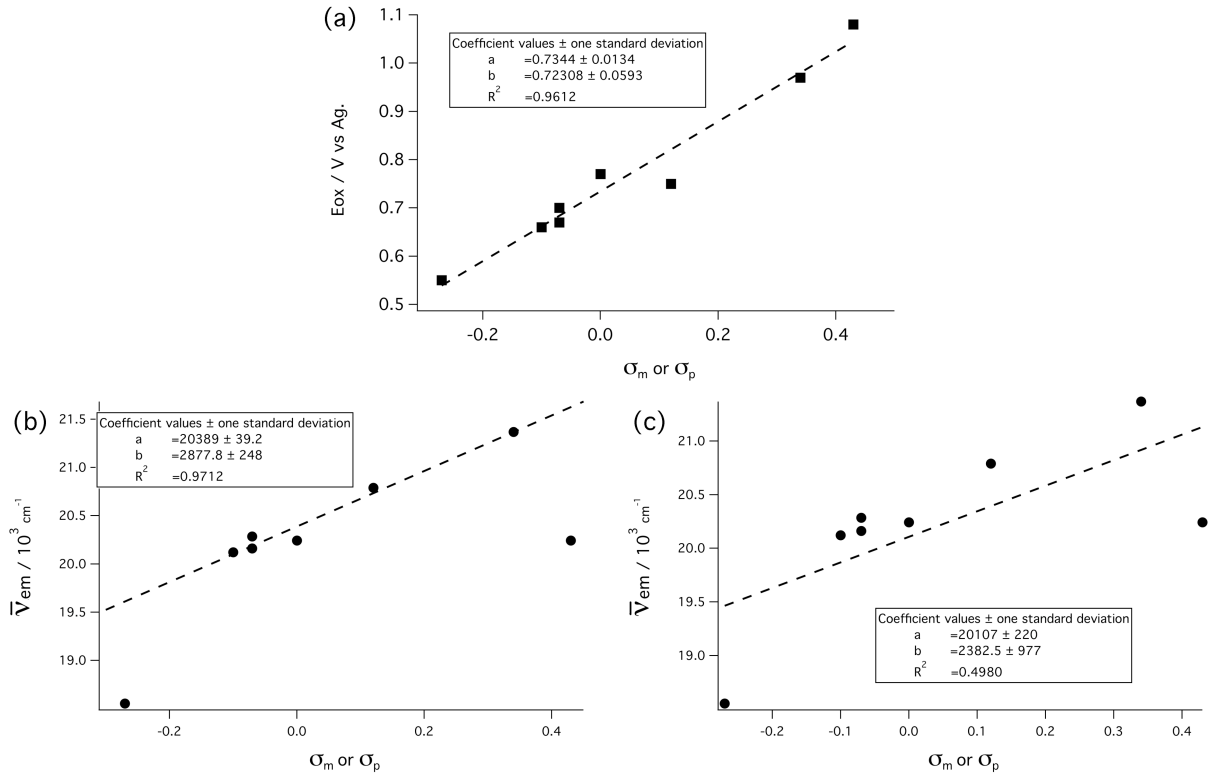

Figure S1. (a) Correlation of E_{OX} with Hammett constants σ ; (b) correlation of emission energy with Hammett constants σ, [Ir(4-CF_3-ppy)$_3$] and [Ir(5-OMe-ppy)$_3$] are not used for the linear regression shown on the graph; (c) correlation of emission energy with Hammett constants σ, [Ir(4-CF_3-ppy)$_3$] and [Ir(5-OMe-ppy)$_3$] are used for the linear regression shown on the graph. Data from ref. 1.

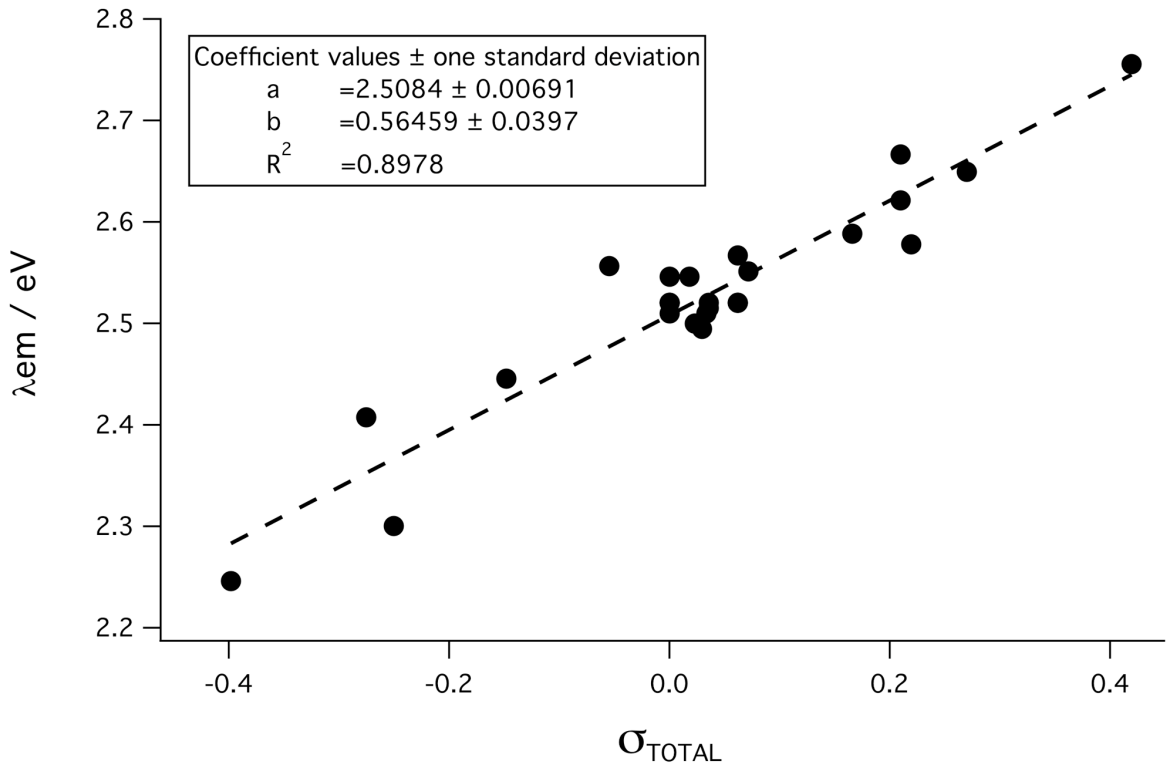

Figure S2. Correlation of λ_{em} with σ_{TOTAL} (Eq. 10) for data used in Figure 1.

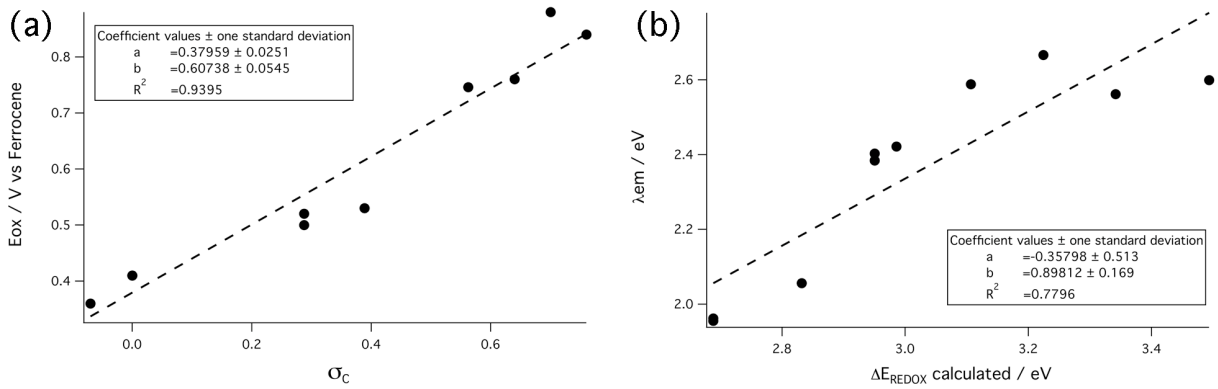

Figure S3. [Ir(R-ppy)$_2$(acac)](a) Correlation of E_{OX} with Hammett constants σ; (b) correlation of λ_{em} with Hammett constants σ.

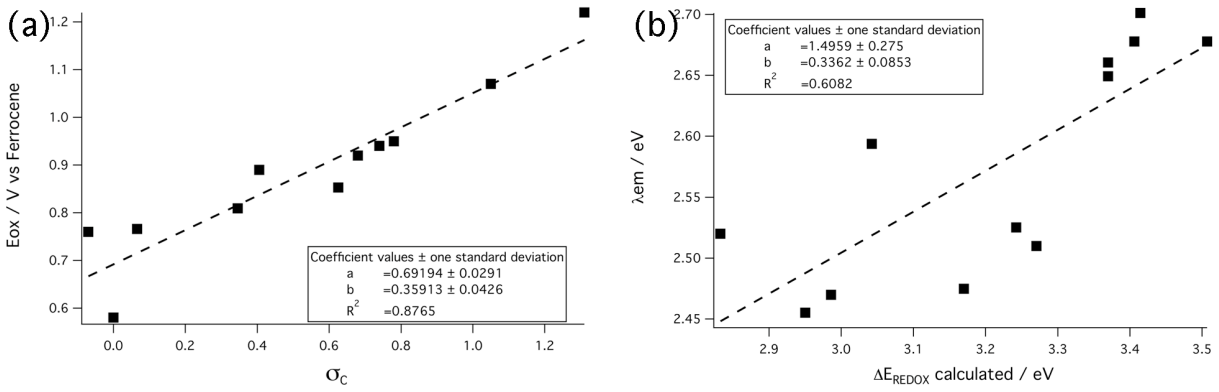

Figure S4. [Ir(R-ppy)$_2$(Pic)](a) Correlation of E_{OX} with Hammett constants σ; (b) correlation of λ_{em} with Hammett constants σ.

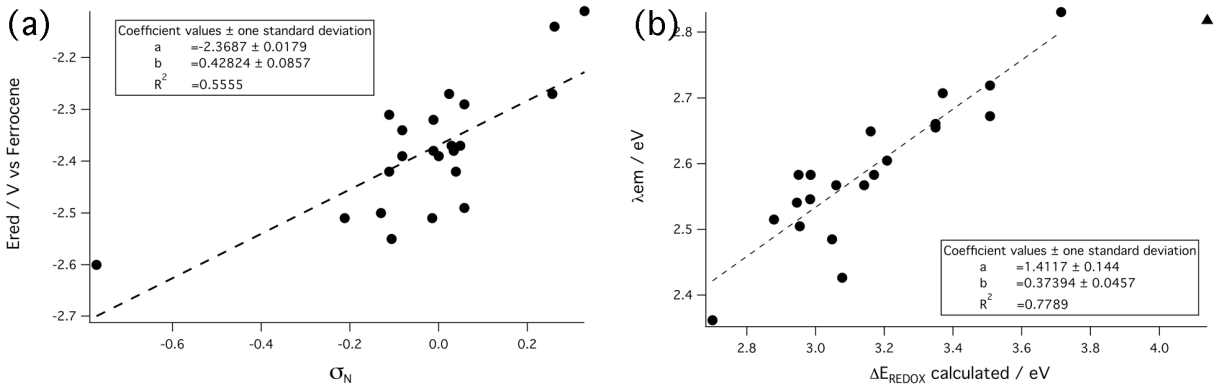

Figure S5. [Pt(R-ppy)(acac)](a) Correlation of E_{OX} with Hammett constants σ; (b) correlation of λ_{em} with Hammett constants σ; data point for [Pt(2-(2,4-difluorophenyl)-4-*N,N*-dimethylaminopyridine)(acac)] is singled out as a triangle and not taken into account for the linear regression.

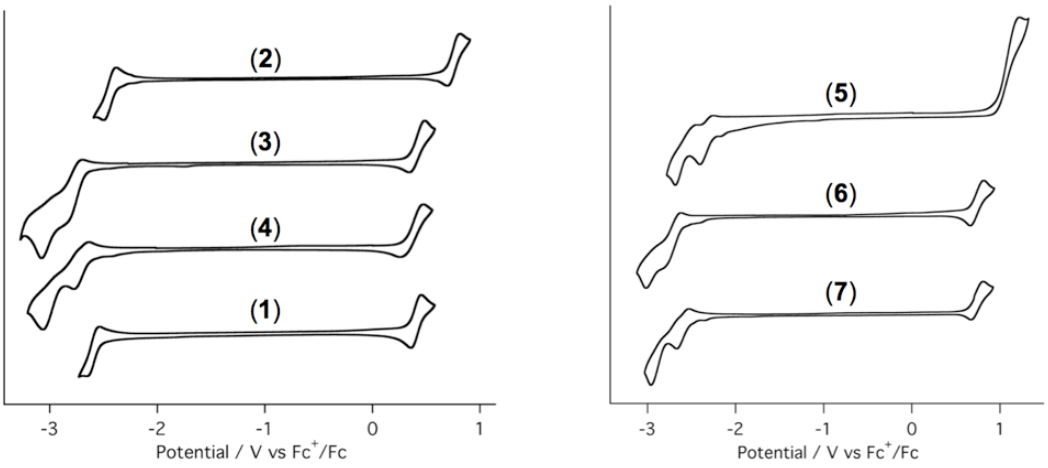

Figure S6. Cyclic voltammograms of (left) **1-4** and (right) **5-7** in dimethylformamide at 1 V s^{-1}.

Table S2. Crystallographic data for **1**, **2**, **3**, **4**, **6**, and **7**.

	1·(CH_2Cl_2)	**2**	**3**·(CH_2Cl_2)	**4**	**6**·(CH_2Cl_2)	**7**
CCDC	964310	964311	964312	964313	964314	964315
empirical formula	$C_{28}H_{25}Cl_2IrN_2O_2$	$C_{27}H_{19}F_4IrN_2O_2$	$C_{32}H_{33}Cl_2IrN_2O_6$	$C_{31}H_{31}IrN_2O_4$	$C_{30}H_{31}Cl_2IrN_4O_6$	$C_{29}H_{29}IrN_4O_4$
formula weight	684.60	671.64	804.70	687.78	806.69	689.76
temperature, K	100(2)	100(2)	100(2) K	100(2)	100(2)	100(2)
wavelength (Å)	0.71073	0.71073	0.71073	0.71073	0.71073	0.71073
crystal system	Triclinic	Monoclinic	Monoclinic	Triclinic	Orthorhombic	Monoclinic
space group	*P*-1	$P2_1/c$	*I*2/*a*	*P*-1	*P*bca	*C*2/*c*
unit cell dimensions						
a (Å)	9.7074(7)	14.2843(12)	23.041(3)	10.0818(16)	30.259(8)	11.1180(13)
b (Å)	9.7515(8)	20.156(3)	10.8791(15)	10.4988(19)	10.1335(11)	22.472(3)
c (Å)	14.0169(11)	17.0651(12)	26.008(5)	13.2307(9)	39.920(10)	12.1117(14)
α (deg)	77.481(7)	90	90	99.755(10)	90	90
β (deg)	81.220(6)	109.041(7)	104.362(9)	92.785(7)	90	90.716(11)
γ (deg)	80.021(7)	90	90	103.058(16)	90	90
volume ($Å^3$)	1266.54(18)	4644.4(9)	6315.6(17)	1339.0(3)	12241(5)	3025.9(7)
Z	2	8	8	2	16	4
density, calcd (g/cm^3)	1.795	1.921	1.693	1.706	1.751	1.514
absorption coefficient (mm^{-1})	5.511	5.810	4.443	5.025	4.587	4.540
F(000)	668	2592	3184	680	6368	1360
crystal size (mm^3)	0.28 x 0.18 x 0.15	0.44 x 0.42 x 0.23	0.50 x 0.46 x 0.20	0.41 x 0.24 x 0.12	0.46 x 0.26 x 0.16	0.48 x 0.13 x 0.12
θ range (deg)	2.85 to 27.42	3.34 to 27.50	3.32 to 27.50	3.34 to 34.00	3.06 to 27.50	3.28 to 30.70
reflections collected	11232	149363	71890	36079	215711	34322
independent reflections	5167	10600	7224	10808	13983	4681
	[R(int) = 0.0219]	[R(int) = 0.0705]	[R(int) = 0.0483]	[R(int) = 0.0293]	[R(int) = 0.0490]	[R(int) = 0.0431]
refinement method	Full-matrix least-squares on F^2	Full-matrix least-squares on F^2	Full-matrix least-squares on F^2	Full-matrix least-squares on F^2	Full-matrix least-squares on F^2	Full-matrix least-squares on F^2
data/restraints/parameters	5167 / 0 / 316	10600 / 0 / 656	7224 / 30 / 416	10808 / 0 / 343	13983 / 31 / 803	4681 / 0 / 174
goodness-of-fit on *F*2	1.089	1.090	1.118	1.115	1.231	1.147
final R indices [I > 2σ(I)]	R1 = 0.0196	R1 = 0.0416	R1 = 0.0238	R1 = 0.0209	R1 = 0.0276	R1 = 0.0254
	wR2 = 0.0492	wR2 = 0.0973	wR2 = 0.0512	wR2 = 0.0439	wR2 = 0.0471	wR2 = 0.0537
R indices (all data)	R1 = 0.0213	R1 = 0.0626	R1 = 0.0333	R1 = 0.0268	R1 = 0.0378	R1 = 0.0301
	wR2 = 0.0496	wR2 = 0.1130	wR2 = 0.0568	wR2 = 0.0468	wR2 = 0.0503	wR2 = 0.0560

Computational details.

Full geometry optimizations of the iridium compounds in their singlet ground state were performed with density functional theory (DFT) using the M06 functional[2] with the relativistic effective core potential and basis set LANL2DZ[3] for the iridium, the TZVP[4] basis set for the remaining atoms, an ultrafine integration grid, and tight geometrical convergence criteria. No symmetry constraints were applied during the geometry optimizations, which were carried out with the Gaussian 09 package.[5] The nature of the stationary points located was further checked by analytical computations of harmonic vibrational frequencies at the same level of theory. Condensed-phase effects were taken into account using a self-consistent reaction-field (SCRF) model in which the solvent is implicitly represented by a dielectric continuum characterized by its relative static dielectric permittivity ε. Within the different approaches that can be followed to calculate the electrostatic potential created by the polarized continuum in the cavity, we have employed the integral equation formalism of the polarizable continuum model (IEFPCM).[6] A relative permittivity of 35.688 (37.219, LR-TDDFT and (U-)DFT) was employed to simulate acetonitrile (*N,N*-dimethylformamide, ionization energy and electron affinity),[5] the solvents used in the experimental work.

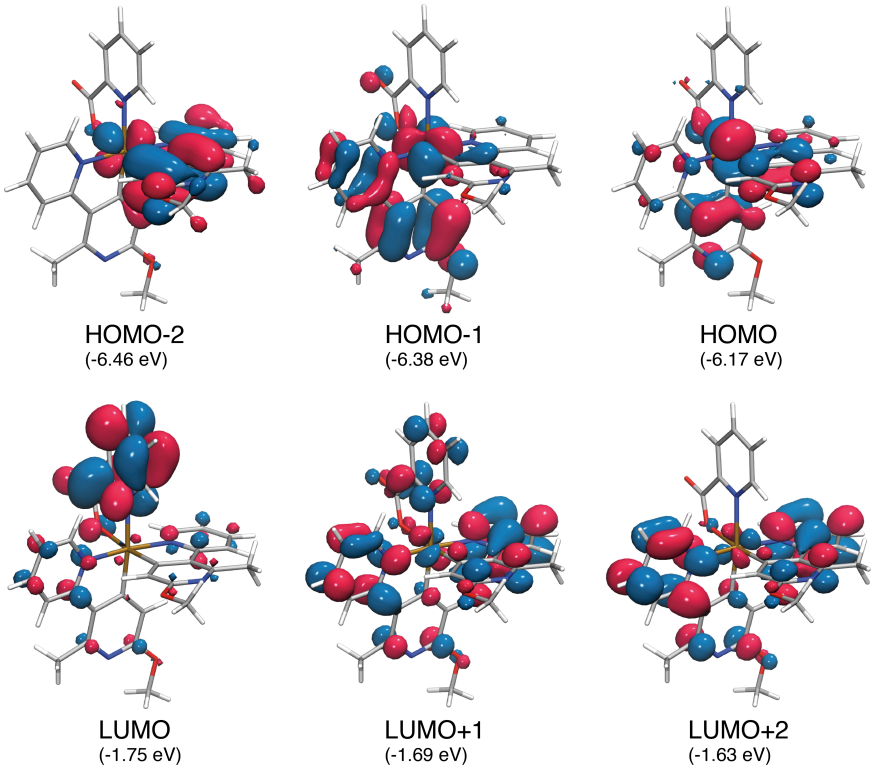

Figure S7. Contour plots of selected Kohn-Sham orbitals for the geometry optimized **EB343**, using DFT/M06/IEF-PCM(ACN). (Isovalue set to 0.03 a.u., orbital energies are provided in eV).

Figure S7 provides the frontier Kohn-Sham (KS) orbitals of **EB343**. The three highest occupied orbitals consist mostly in 5d(Ir) orbitals with contributions from the 2,3'-pyridine ligands. The first three unoccupied orbitals are close in energy and are delocalized over the ancillary and the 6'-methoxy-2'-methyl-2,3'-bipyridine ligands.

Vertical electronic transitions from the ground state geometry of **EB343** were computed within linear-response time-dependent density functional theory (LR-TDDFT), using the same functional and basis sets (non-equilibrium solvation[7] has been used for the LR-TDDFT calculations of absorption spectra). Interestingly, the first allowed transition (3.32 eV, f=0.014, GS->S_1) possesses a HOMO -> LUMO+1 character (87%), while the transition to the first triplet (2.89 eV, GS->T_1) is composed by several occupied to virtual orbital transitions with no strong dominant contribution.

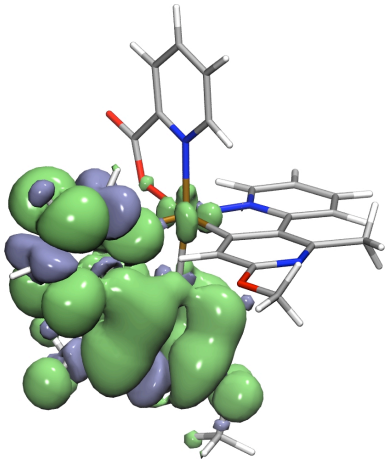

Figure S8. Contour plots of the spin density of **EB343** at its optimized T_1 geometry, using U-DFT/M05-2X/IEF-PCM(ACN). (Isovalue set to 0.0008 a.u.).

To gain insights into the phosphorescence behavior of the different iridium compounds, we optimized the geometry of the first triplet state using unrestricted DFT (U-DFT) with the same basis set as described before. As suggested by a recent work,[8] we used the *xc*-functional M05-2X[9] for this task, due to its excellent performance for the emission spectra for a series of iridium-based compounds. At the minimum energy structure, we computed the difference in energy between the triplet (T_1) and singlet (S_0) with the inclusion of implicit solvent and obtained an estimation of the first phosphorescence band. In addition, the adiabatic energy differences were computed by taking the difference between the energy at the optimized T_1 geometry and the energy at the optimized GS geometry. The character of the T_1 state can be described as being mostly of ligand-centered type (see Figure S8 for a spin density plot at the T_1 optimized geometry). The computed vertical electronic energy difference between the T_1 and the GS (at the

T_1 geometry) lies at 2.41 eV for **EB343** and 2.65 eV for **FIrPic**. We note that the geometry of a low-lying triplet state, formed by populating an orbital located on the pic ligand, was also optimized. At its optimized geometry, this triplet state lies at 0.1 eV from the corresponding geometry optimized T_1 state.

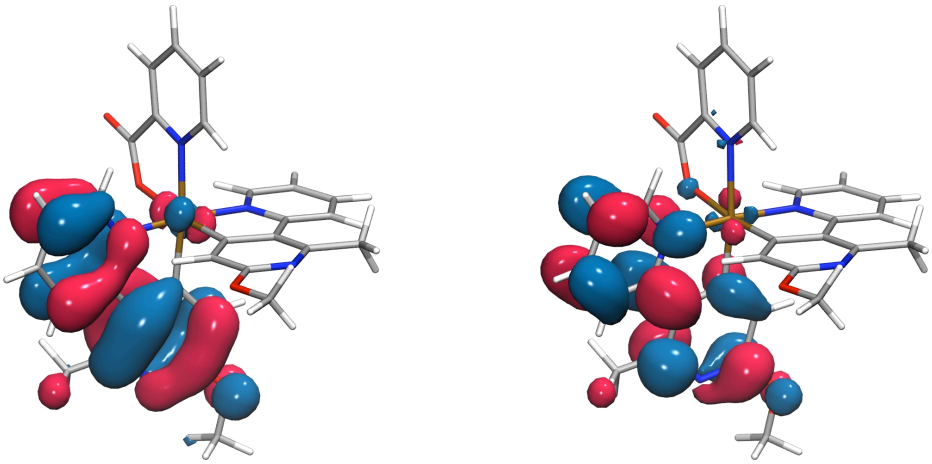

Figure S9. Contour plots of selected Kohn-Sham orbitals, HOMO (left) and LUMO (right), at the geometry optimized T_1 state of **EB343**, using LR-TDDFT/M05-2X/IEF-PCM(ACN). (Isovalue set to 0.03 a.u.).

Geometry optimization of **EB343** in its T_1 electronic state was further undertaken using LR-TDDFT/M05-2X/IEF-PCM(ACN) with an ultrafine grid and the default convergence criteria in Gaussian09. The LR-TDDFT optimized T_1 geometry exhibits a similar character as the one obtained from the U-DFT optimization, with a dominant HOMO->LUMO contribution (91%) (Figure S9).

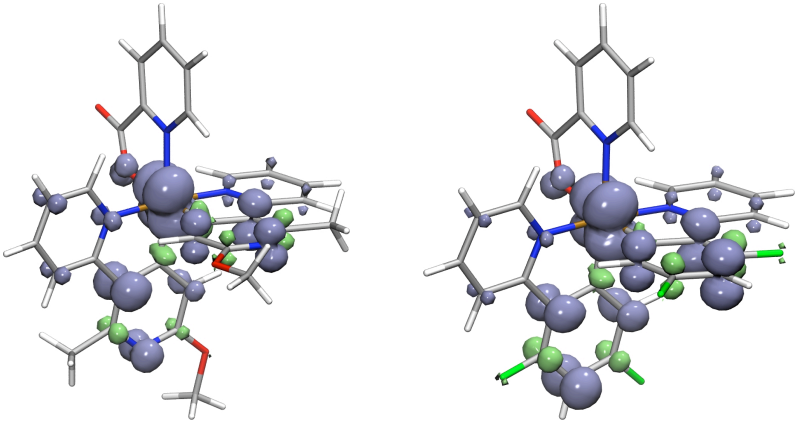

Figure S10. Contour plots of the spin density of **EB343**$^+$ (left) and **FIrPic**$^+$ (right) at their respective optimized GS geometry, using U-DFT/M06/IEF-PCM(DMF). (Isovalue at 0.003 a.u.).

The vertical IE of **EB343** was obtained by computing the energy of the cationic species **EB343**$^{+}$ at the ground state optimized geometry of **EB343**, using an unrestricted U−DFT/M06/IEF-PCM(DMF) calculations with the same parameters as described above, and subtracting it from the energy of the geometry optimized **EB343** (DFT/M06/IEF-PCM(DMF)). **EB343** shows a vertical IE of 5.89 eV, close to the 5.78 eV of FIrPic computed in the same way. The spin density resulting from this calculation is mostly localized on the Ir center, with some contributions from the 2,3'-bipyridine ligands (Figure S10, left), a localization similar to the spin density of **FIrPic**$^{+}$ (Figure S10, right).

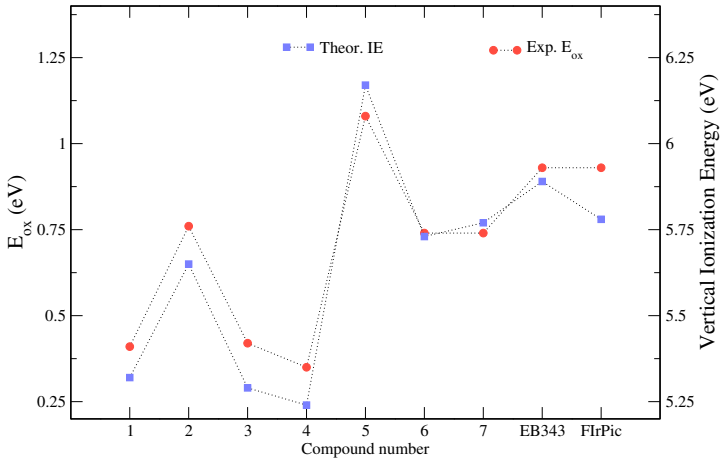

Figure S11. Comparison between computed vertical ionization energy ((U-)DFT/M06/IEF-PCM(DMF)) and experimental oxidation potential for the complete series of iridium complexes.

We note that the computed vertical IEs for the different iridium compounds proposed in this work follow closely the trend in oxidation potential obtained experimentally (Figure S11). Based on the same level of theory, the vertical ionization potential and electron affinity were computed for the freely optimized 6'-methoxy-2'-methyl-2,3'-bipyridine and 2,4-difluorophenylpyridine ligands (from their anionic state). We observed that both their vertical ionization potential (4.11 eV vs 4.17 eV, respectively) and electron affinity (−0.95 eV in both cases) are almost degenerate, in agreement with the experimental predictions.

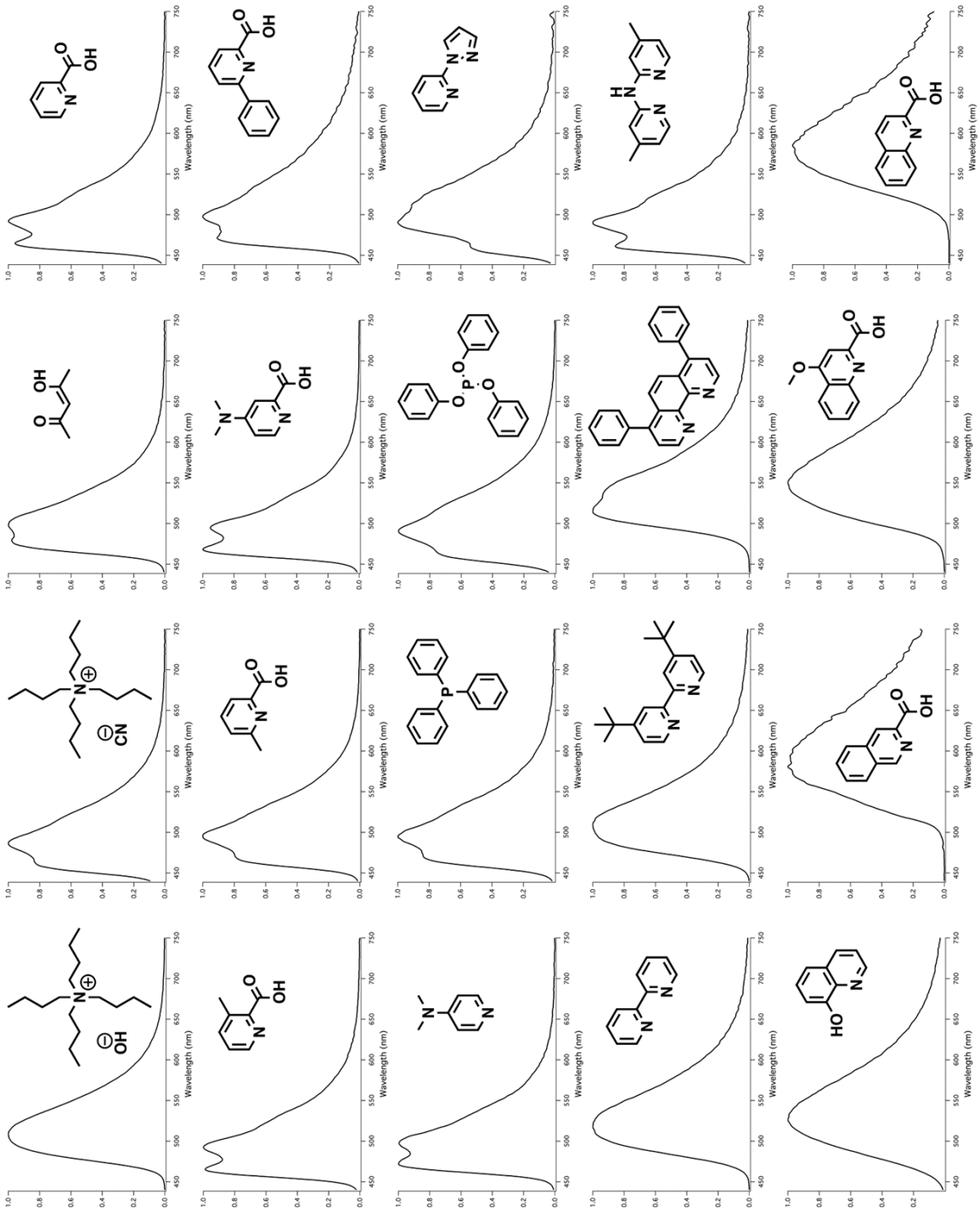

Figure S12. Emission spectra from screening procedure with $[Ir(L7)_2(\mu\text{–}Cl)]_2$

2-(2,4-Dimethoxyphenyl)-pyridine (L3). A flask was charged with 2,4-dimethoxyphenyl-boronic acid (98%, 1.00 g, 5.38 mmol), 2-bromopyridine (99%, 0.88 g, 5.38 mmol, 1.0 eq.) and $Pd(PPh_3)_4$ (97%, 0.32 g, 3.02 x 10^{-4} mol, 5%). The solids were degassed with nitrogen and dissolved in a 3:7 mixture of 2M aqueous Na_2CO_3 and THF (8 and 19 mL, respectively). After further degassing the mixture was warmed up to 80 °C and refluxed for 18 hours under vigorous stirring. Then it was cooled down to RT and extracted with CH_2Cl_2 and water. The organic layer was decanted, dried over $MgSO_4$, filtered and evaporated to dryness. Purification by chromatography, (1) silica prepared in hexane / THF 80:20, isocratic elution with hexane / THF 80:20, and (2) silica prepared in hexane / CH_2Cl_2 / Et_2O 50:30:20, isocratic elution with hexane / CH_2Cl_2 / Et_2O 50:30:20, afforded **L3** as a colorless oil (0.82 g, 71%). ^{1}H NMR ($CDCl_3$, 400 MHz): δ 8.64 (broad ddd, 1H, J = 4.8 Hz); 7.78 (d, 1H, J = 8.0 Hz); 7.75 (d, 1H, J = 8.5 Hz); 7.64 (ddd, 1H, J = 7.7, 1.9 Hz); 7.13 (dd, 1H, J = 4.8, 2.6 Hz); 6.60 (dd, 1H, J = 8.3, 2.3 Hz); 6.54 (d, 1H, J = 2.3 Hz); 3.84 (s, 3H); 3.83 (s, 3H). Data are identical to the published ones.[10]

2-(4-Methoxy-2-methylphenyl)-pyridine (L4). A flask was charged with 2,4-dimethoxyphenyl-boronic acid (98%, 1.00 g, 2.36 mmol), 2-bromopyridine (99%, 0.94 g, 2.36 mmol, 1.0 eq.) and $Pd(PPh_3)_4$ (97%, 0.35 g, 1.95 x 10^{-4} mol, 5%). The solids were degassed with nitrogen and dissolved in a 3:7 mixture of 2M aqueous Na_2CO_3 and THF (9 and 20 mL, respectively). After further degassing the mixture was warmed up to 80 °C and refluxed for 18 hours under vigorous stirring. Then it was cooled down to RT and extracted with CH_2Cl_2 and water. The organic layer was decanted, dried over $MgSO_4$, filtered and evaporated to dryness. Purification by chromatography, (1) silica prepared in hexane / Et_2O 70:30, isocratic elution with hexane / Et_2O 70:30, and (2) silica prepared in hexane / EtOAc 70:30, isocratic elution with hexane / EtOAc 70:30, afforded **L4** as a colorless oil (1.07 g, 90%). ^{1}H NMR ($CDCl_3$, 400 MHz): δ 8.65 (broad ddd, 1H, J = 4.1 Hz); 7.67 (ddd, 1H, J = 7.7, 1.6 Hz); 7.33 (m, 2H); 7.16 (ddd, 1H, J = 4.1, 1.2 Hz); 6.80 (m, 2H); 3.82 (s, 3H); 2.36 (s, 3H). Data are identical to the published ones.[11]

2',6'-Difluoro-2,3'-bipyridine (L5). A flask was charged with 2,6-difluoro-3-pyridinyl-boronic acid (96%, 1.00 g, 6.04 mmol), 2-bromopyridine (99%, 0.98 g, 6.04 mmol, 1.0 eq.) and $Pd(PPh_3)_4$ (97%, 360 mg, 3.02 x 10^{-4} mol, 5%). The solids were degassed with nitrogen and dissolved in a 3:7 mixture of 2M aqueous Na_2CO_3 and THF (9 and 21 mL, respectively). After further degassing the mixture was warmed up to 80 °C and refluxed for 18 hours under vigorous stirring. Then it was cooled down to RT and extracted with CH_2Cl_2 and water. The organic layer was decanted, dried over $MgSO_4$, filtered and evaporated to dryness. Purification by chromatography, silica prepared in hexane / Et_2O 80:20, isocratic elution with hexane / Et_2O 80:20, afforded **L5** as a white crystalline solid (0.99 g, 85%). ^{1}H NMR ($CDCl_3$, 400 MHz): δ 8.70 (ddd, 1H, J = 4.8, 1.8, 1.2 Hz); 8.67 (ddd, 1H, J = 8.0, 6.4, 1.6 Hz); 7.85 (m, 1H, J = 8.0, 3.2, 1.2 Hz); 7.78 (ddd, 1H, J = 8.2, 6.4, 1.8 Hz); 7.29 (ddd, 1H, J = 4.8, 2.6, 1.2 Hz); 6.96 (ddd, 1H, J = 8.2, 3.2, 1.6 Hz). Data are identical to the published ones.[12]

2',6'-Dimethoxy-2,3'-bipyridine (L6). *2,6-Dimethoxy-3-pyridinyl-boronic acid*. Anhydrous diisopropylamine (99.5%, 2.2 mL, 15.4 mmol, 1.1 eq.) was charged in an oven-dried two-necked flask, degassed with nitrogen and dissolved in anhydrous THF (30 mL - 2 mL/mmol). The solution was cooled down to -10 °C and *n*-BuLi (2.5M, 6.8 mL, 16.8 mmol, 1.2 eq.) was added drop wise. After 30 minutes of stirring at 0 °C, it was cooled down to -78 °C. 2,6-Dimethoxy-pyridine (98%, 2.0 g, 14.0 mmol) was added over a 30-min period and the resulting mixture was stirred during 3 hours at -78 °C. Then $B(O^iPr)_3$ (98%, 4.3 mL, 18.2 mmol, 1.3 eq.) was added and the solution was allowed to warm to RT overnight. Water (150 mL) was added and the organic was removed under vacuum. The remaining solution was filtered and then acidified to pH ~ 6 using 37% HCl to promote precipitation. The solid was collected by filtration and dried under vacuum (2.06 g, 80%). ^{1}H NMR (d_6-DMSO, 400 MHz): δ 7.87 (d, 1H, J = 7.9 Hz); 7.54 (s, 2H); 6.37 (d, 1H, J = 7.9 Hz); 3.90 (s, 3H); 3.87 (s, 3H); 3.32 (s, 3H). Data are identical to the published ones.[13] *2',6'-Dimethoxy-2,3'-bipyridine*. A two-necked flask was charged with 2,6-dimethoxy-3-pyridinyl-boronic acid (1.00 g, 5.46 mmol), 2-bromopyridine (99%, 0.87 g, 5.46

mmol, 1.0 eq.) and $Pd(PPh_3)_4$ (97%, 325 mg, 2.74 x 10^{-4} mmol, 5%). The solids were degassed with nitrogen and dissolved in a 3:7 mixture of 2M aqueous Na_2CO_3 and PhMe (8 + 19 mL, respectively). After further degassing the mixture was warmed up to 80 °C and refluxed for 18 hours under vigorous stirring. Then it was cooled down to RT and extracted with CH_2Cl_2 and water. The organic layer was decanted, dried over $MgSO_4$, filtered and evaporated to dryness. Purification by chromatography, (1) silica prepared in hexane / Et_2O 80:20, elution with hexane / Et_2O 80:20, (2) silica prepared in CH_2Cl_2 / Et_2O 95:5, elution with CH_2Cl_2 / Et_2O 95:5, afforded **L6** as a white solid (605 mg, 51%). ^{1}H NMR ($CDCl_3$, 400 MHz, 25 °C): δ 8.63 (ddd, 1H, J = 4.8, 1.8, 1.2 Hz); 8.23 (d, 1H, J = 8.2 Hz); 7.93 (broad d, 1H, J = 8.0 Hz); 7.67 (ddd, 1H, J = 7.6, 1.9 Hz); 7.13 (ddd, 1H, J = 7.5, 4.8, 1.2 Hz); 6.43 (d, 1H, J = 8.2 Hz); 4.02 (s, 3H); 3.96 (s, 3H). Data are identical to the published ones.[14]

6'-Methoxy-2'-methyl-2,3'-bipyridine (L7). *3-Bromo-6-methoxy-2-methyl-pyridine*. 2-Methoxy-6-methyl-pyridine (98%, 2.00 g, 15.9 mmol) was suspended in 0.15 M aqueous Na_2HPO_4 (32 mL) and bromine (2.54 g, 15.9 mmol, 1.0 eq.) was added drop wise. The resulting solution was stirred for 4 hours at RT. Then it was partitioned between CH_2Cl_2 and water. The organic layer was decanted, washed with 10% aqueous NaOH (32 mL), then dried over $MgSO_4$, filtered and evaporated to dryness. Purification was achieved by distillation under reduced pressure. The compound (2.06 g, 95% overall yield) was isolated as a mixture of 2 isomers, the desired 3-bromo-6-methoxy-2-methylpyridine (95%) contaminated by 5-bromo-6-methoxy-2-methylpyridine (5%). ^{1}H NMR ($CDCl_3$, 400 MHz): δ 7.59 (d, 1H, J = 8.6 Hz); 6.44 (d, 1H, J = 8.6 Hz); 3.87 (s, 3H); 2.52 (s, 3H). Impurity: δ 7.62 (d, 1H, J = 7.6 Hz); 6.59 (d, 1H, J = 7.6 Hz); 3.97 (s, 3H); 2.39 (s, 3H). Data are identical to the published ones.[15] *6-Methoxy-2-methyl-3-pyridinyl-boronic acid*. The mixture and 3- and 5-bromo-6-methoxy-2-methylpyridine (2.00 g, 10.0 mmol) was charged in an oven-dried two-necked flask, degassed with nitrogen, dissolved in anhydrous THF (20 mL - 2 mL/mmol) and cooled down to -78 °C. *n*-BuLi (2.5M, 4.4 mL, 11.0 mmol, 1.1 eq.) was added over a 30-min period and the mixture was reacted for 3 hours at -78

°C. After addition of $B(O^iPr)_3$ (98%, 3.5 mL, 15.0 mmol, 1.5 eq.), it was reacted for another 5 hours at -78 °C and then allowed to warm to RT overnight. AcOH (1.5 mL) and water (4.0 mL) were added and the mixture was stirred for another 2 hours at RT. After decantation, the organic layer was evaporated to dryness (bath at 50 °C) with addition of ^{t}BuOH (3 x 15.0 mL) aliquots. The white solid obtained was triturated with Et_2O, filtered and dried under vacuum affording the title compound (1.52 g, 92%). ^{1}H NMR (CD_3OD, 400 MHz): δ 7.83 (broad s, 1H, J = 8.0 Hz); 6.56 (d, 1H, J = 8.0 Hz); 3.83 (s, 3H); 2.44 (s, 3H). Data are identical to the published ones.[15] *6'-Methoxy-2'-methyl-2,3'-bipyridine*. A two-necked flask was charged with 6-methoxy-2-methyl-3-pyridinyl-boronic acid (1.00 g, 5.96 mmol), 2-bromopyridine (99%, 0.96 g, 5.96 mmol, 1.0 eq.) and $Pd(PPh_3)_4$ (97%, 355 mg, 3.00 x 10^{-4} mol, 5%). The solids were degassed with nitrogen and dissolved in a 3:7 mixture of 2M aqueous Na_2CO_3 and PhMe (12 and 26 mL, respectively). After further degassing the mixture was warmed up to 80 °C and refluxed for 18 hours under vigorous stirring. Then it was cooled down to RT and extracted with CH_2Cl_2 and water. The organic layer was decanted, dried over $MgSO_4$, filtered and evaporated to dryness. Purification by chromatography, (1) silica prepared in CH_2Cl_2 / Et_2O 85:15, gradient elution from CH_2Cl_2 / Et_2O 85:15 to 70:30, (2) silica prepared in hexane / Et_2O 60:40, elution with hexane / Et_2O 60:40, afforded **L7** as a colorless oil (635 mg, 53%). ^{1}H NMR ($CDCl_3$, 400 MHz): δ 8.66 (dd, 1H, J = 4.9, 1.9 Hz); 7.71 (ddd, 1H, J = 7.8, 7.6, 1.9 Hz); 7.65 (d, 1H, J = 8.3 Hz); 7.37 (d, 1H, J = 7.8, 1.0 Hz); 7.21 (ddd, 1H, J = 7.6, 4.9, 1.0 Hz); 6.64 (d, 1H, J = 8.3 Hz); 3.95 (s, 3H); 2.51 (s, 3H). ^{13}C NMR ($CDCl_3$, 100 MHz): *d* 163.32, 158.50, 154.10, 149.68, 140.53, 136.42, 128.87, 124.33, 121.81, 107.84, 53.68, 23.35. ESI-TOF HRMS: MH^+ *m/z*: calc. 201.10128 found 201.1031. Anal. calcd. for $C_{12}H_{12}N_2O$: C, 71.98; H, 6.04; N, 13.99. Found C, 71.96; H, 6.10; N, 14.11.

General method for the synthesis of phenylpyridine chloro-bridged dimer complexes. $IrCl_3.xH_2O$ (500 mg, 1.42 mmol) was suspended in 10 mL of 2-ethoxyethanol and 4 mL of water. The suspension was filled with nitrogen by 3 cycles vacuum/nitrogen. The ligand L (3.12

mmol, 2.2 equiv) was added, and 2 mL of 2-ethoxyethanol was used for rinsing. The mixture was filled again with nitrogen by 3 cycles vacuum/nitrogen. The flask was sealed and heated at 130 °C overnight. Then it was cooled down to room temperature, and water was added to further precipitation. The solid was filtered, washed with water, then with methanol, and dried to afford the chloro-bridged iridium dimer $[Ir(L)_2(\mu\text{–}Cl)]_2$.

$[Ir(L3)_2(\mu\text{–}Cl)]_2$. L was 2-(2,4-dimethoxyphenyl)-pyridine (L3). The chloro-bridged iridium dimer $[Ir(L3)_2(\mu\text{-}Cl)]_2$ was obtained as an yellow solid (808 mg, 87%). ^{1}H NMR ($CDCl_3$, 400 MHz): δ 9.18 (d, 4H, J = 5.1 Hz); 8.54 (d, 4H, J = 8.3 Hz); 7.59 (ddd, 4H, J = 7.3, 1.5 Hz); 6.58 (ddd, 4H, J = 5.7, 1.3 Hz); 5.89 (d, 4H, J = 1.9 Hz); 5.05 (d, 4H, J = 2.2 Hz); 3.81 (s, 12H); 3.30 (s, 12H).

$[Ir(L4)_2(\mu\text{–}Cl)]_2$. L was 2-(4-methoxy-2-methylphenyl)-pyridine (L4). The chloro-bridged iridium dimer $[Ir(L4)_2(\mu\text{–}Cl)]_2$ was obtained as an orange solid (735 mg, 83%). ^{1}H NMR ($CDCl_3$, 400 MHz): δ 9.29 (d, 4H, J = 5.8 Hz); 7.96 (d, 4H, J = 8.2 Hz); 7.65 (ddd, 4H, J = 7.6 Hz); 6.65 (ddd, 4H, J = 6.6 Hz); 6.11 (s, 4H); 5.21 (d, 4H, J = 1.2 Hz); 3.32 (s, 12H); 3.30 (s, 12H).

General method for the synthesis of acetylacetonate complexes. Sodium acetylacetonate (98%, 4.0 equiv.) was dissolved in CH_2Cl_2 / MeOH (30 and 10 mL, respectively), and this solution was added to a suspension of the corresponding dimer in CH_2Cl_2 (10 mL). The solution was gently refluxed at 40 °C under nitrogen overnight. After cooling down to room temperature, the solution was evaporated to dryness. The crude material was dissolved in pure CH_2Cl_2 and filtered over a pad of neutral silica. The volume of the solution was reduced under vacuum and the main fraction was slowly precipitated with hexane. The suspension was filtered off, washed with hexane, and dried under vacuum to afford $[Ir(L)_2(acac)]$ complexes as solids.

$[Ir(L3)_2(acac)]$ (3). Using $[Ir(L3)_2(\mu\text{–}Cl)]_2$ (250 mg, 1.91 x 10^{-4} mol), complex **3** was obtained as a yellow solid (154 mg, 56%). ^{1}H NMR ($CDCl_3$, 400 MHz): δ 8.51 (broad d, 2H, J = 8.3 Hz); 8.44 (broad dd, 2H, J = 5.7, 1.6 Hz); 7.60 (ddd, 2H, J = 7.5, 1.8 Hz); 6.95 (ddd, 2H, J = 5.7, 1.5

Hz); 5.95 (d, 2H, J = 2.2 Hz); 5.38 (d, 2H, J = 2.2 Hz); 5.16 (s, 1H); 3.85 (s, 6H); 3.45 (s, 6H); 1.75 (s, 6H). ESI-TOF HRMS: MH^+ *m/z*: calc. 721.1891 found 721.1907. Anal. calcd. for $C_{31}H_{31}IrN_2O_6$: C, 51.73; H, 4.34; N, 3.89. Found C, 51.45; H, 4.38; N, 3.95.

[Ir(L4)$_2$(acac)] (4). Using $[Ir(L4)_2(\mu\text{–}Cl)]_2$ (250 mg, 2.00 x 10^{-4} mol), complex **4** was obtained as an orange solid (123 mg, yield 45%). ^{1}H NMR ($CDCl_3$, 400 MHz): δ 9.22 (dd, 2H, J = 5.7, 1.5 Hz); 7.96 (d, 2H, J = 8.5 Hz); 7.64 (ddd, 2H, J = 8.5, 1.8 Hz); 7.00 (ddd, 2H, J = 5.7, 1.0 Hz); 6.16 (d, 2H, J = 2.6 Hz); 5.58 (d, 2H, J = 2.6 Hz); 5.61 (s, 1H); 3.47 (s, 6H); 2.64 (s, 6H); 1.74 (s, 6H). ESI-TOF HRMS: MH^+ *m/z*: calc. 688.1915 found 688.1914. Anal. calcd. for $C_{31}H_{31}IrN_2O_4$: C, 54.13; H, 4.54; N, 4.07. Found C, 54.14; H, 4.43; N, 4.02.

[Ir(L5)$_2$(acac)] (5). Using $[Ir(L5)_2(\mu\text{–}Cl)]_2$ (250 mg, 2.05 x 10^{-4} mol), complex **5** was obtained as a pale yellow solid (188 mg, 68%). ^{1}H NMR ($CDCl_3$, 400 MHz): δ 8.43 (ddd, 2H, J = 5.8, 1.5, 0.6 Hz); 8.27 (ddd, 2H, J = 8.3,1.3, 0.6 Hz); 7.90 (ddd, 2H, J = 8.3, 1.5 Hz); 7.30 (ddd, 2H, J = 5.8, 1.3 Hz); 5.62 (t, 2H, J = 1.8 Hz); 5.28 (s, 1H); 1.82 (s, 6H). ^{19}F NMR ($CDCl_3$, 400 MHz): δ –69.76 (d, J = 9.8 Hz); –71.53 (dd, J = 9.8, 1.8 Hz). ESI-TOF HRMS: MH^+ *m/z*: calc. 675.0996 found 675.1006. Anal. calcd. for $C_{25}H_{17}F_4IrN_4O_2$: C, 44.57; H, 2.54; N, 8.32. Found C, 44.47; H, 2.47; N, 8.17.

[Ir(L6)$_2$(acac)] (6). Using $[Ir(L6)_2(\mu\text{–}Cl)]_2$ (250 mg, 1.90 x 10^{-4} mol), complex **6** was obtained as a yellow solid (207 mg, 76%). ^{1}H NMR ($CDCl_3$, 400 MHz): δ 8.43 (broad ddd, 2H, J = 8.3 Hz); 8.36 (ddd, 2H, J = 5.7, 1.6, 0.6 Hz); 7.66 (ddd, 2H, J = 8.3, 1.6 Hz); 6.99 (ddd, 2H, J = 5.8, 0.9 Hz); 5.24 (s, 2H); 5.19 (s, 1H); 3.98 (s, 6H); 3.69 (s, 6H); 1.76 (s, 6H). ESI-TOF HRMS: MH^+ *m/z*: calc. 723.1796 found 723.1792. Anal. calcd. for $C_{29}H_{29}IrN_4O_6$: C, 48.26; H, 4.05; N, 7.76. Found C, 47.88; H, 4.03; N, 7.55.

[Ir(L7)$_2$(acac)] (7). Using $[Ir(L7)_2(\mu\text{–}Cl)]_2$ (250 mg, 2.00 x 10^{-4} mol), complex **7** was obtained as a yellow solid (180 mg, 65%). ^{1}H NMR ($CDCl_3$, 400 MHz): δ 8.48 (ddd, 2H, J = 5.7, 1.6 Hz); 7.98 (broad ddd, 2H, J = 8.5 Hz); 7.74 (ddd, 2H, J = 8.5, 1.8 Hz); 7.08 (ddd, 2H, J = 5.7,

1.2 Hz); 5.43 (s, 2H); 5.20 (s, 1H); 3.71 (s, 6H); 2.74 (s, 6H); 1.76 (s, 6H). ESI-TOF HRMS: MH^+ *m/z*: calc. 691.1898 found 691.1876. Anal. calcd. for $C_{29}H_{29}IrN_4O_4$: C, 50.50; H, 4.24; N, 8.12. Found C, 50.45; H, 4.30; N, 8.07.

References for SI section

1. K. Dedeian, P. I. Djurovich, F. O. Garces, G. Carlson and R. J. Watts, *Inorg. Chem.*, 1991, **30**, 1685.
2. Y. Zhao and D. G. Truhlar, *Theor. Chem. Acc.*, 2008, **120**, 215.
3. P. J. Hay and W. R. Wadt, *J. Chem. Phys.*, 1985, **82**, 299.
4. A. D. McLean and G. S. Chandler, *J. Chem. Phys.*, 1980, **72**, 5639.
5. M. J. Frisch, G. W. Trucks, H. B. Schlegel, G. E. Scuseria, M. A. Robb, J. R. Cheeseman, G. Scalmani, V. Barone, B. Mennucci, G. A. Petersson, H. Nakatsuji, M. Caricato, X. Li, H. P. Hratchian, A. F. Izmaylov, J. Bloino, G. Zheng, J. L. Sonnenberg, M. Hada, M. Ehara, K. Toyota, R. Fukuda, J. Hasegawa, M. Ishida, T. Nakajima, Y. Honda, O. Kitao, H. Nakai, T. Vreven, J. Montgomery, J. A., J. E. Peralta, F. Ogliaro, M. Bearpark, J. J. Heyd, E. Brothers, K. N. Kudin, V. N. Staroverov, R. Kobayashi, J. Normand, K. Raghavachari, A. Rendell, J. C. Burant, S. S. Iyengar, J. Tomasi, M. Cossi, N. Rega, J. M. Millam, M. Klene, J. E. Knox, J. B. Cross, V. Bakken, C. Adamo, J. Jaramillo, R. Gomperts, R. E. Stratmann, O. Yazyev, A. J. Austin, R. Cammi, C. Pomelli, J. W. Ochterski, R. L. Martin, K. Morokuma, V. G. Zakrzewski, G. A. Voth, P. Salvador, J. J. Dannenberg, S. Dapprich, A. D. Daniels, Ö. Farkas, J. B. Foresman, J. V. Ortiz, J. Cioslowski and D. J. Fox, *Gaussian 09, Revision A.02*, Gaussian, Inc., Wallingford CT, 2009.
6. J. Tomasi, B. Mennucci and R. Cammi, *Chem. Rev.*, 2005, **105**, 2999.
7. G. Scalmani, M. J. Frisch, B. Mennucci, J. Tomasi, R. Cammi and V. Barone, *J. Chem. Phys.*, 2006, **124**, 094107.
8. K. Swiderek and P. Paneth, *J. Phys. Org. Chem.*, 2009, **22**, 845.
9. Y. Zhao, N. E. Schultz and D. G. Truhlar, *J. Chem. Theory and Comput.*, 2006, **2**, 364.
10. P. C. Astles, C. Brealey, T. J. Brown, V. Facchini, C. Handscombe, N. V. Harris, C. McCarthy, I. M. McLay, B. Porter, A. G. Roach, C. Sargent, C. Smith and R. J. A. Walsh, *J. Med. Chem.*, 1998, **41**, 2732.
11. A. G. Fang, J. V. Mello and N. S. Finney, *Org. Lett.*, 2003, **5**, 967.
12. S. J. Lee, K. M. Park, K. Yang and Y. Kang, *Inorg. Chem.*, 2009, **48**, 1030.
13. A. E. Smith, K. M. Clapham, A. S. Batsanov, M. R. Bryce and B. Tarbit, *Eur. J. Org. Chem.*, 2008, 1458.
14. T. N. Nguyen, N. Marquise, F. Chevallier and F. Mongin, *Chem. Eur. J.*, 2011, **17**, 10405.
15. P. J. Gilligan, T. Clarke, L. He, S. Lelas, Y.-W. Li, K. Heman, L. Fitzgerald, K. Miller, G. Zhang, A. Marshall, C. Krause, J. F. McElroy, K. Ward, K. Zeller, H. Wong, S. Bai, J. Saye, S. Grossman, R. Zaczek, S. P. Arneric, P. Hartig, D. Robertson and G. Trainor, *J. Med. Chem.*, 2009, **52**, 3084.

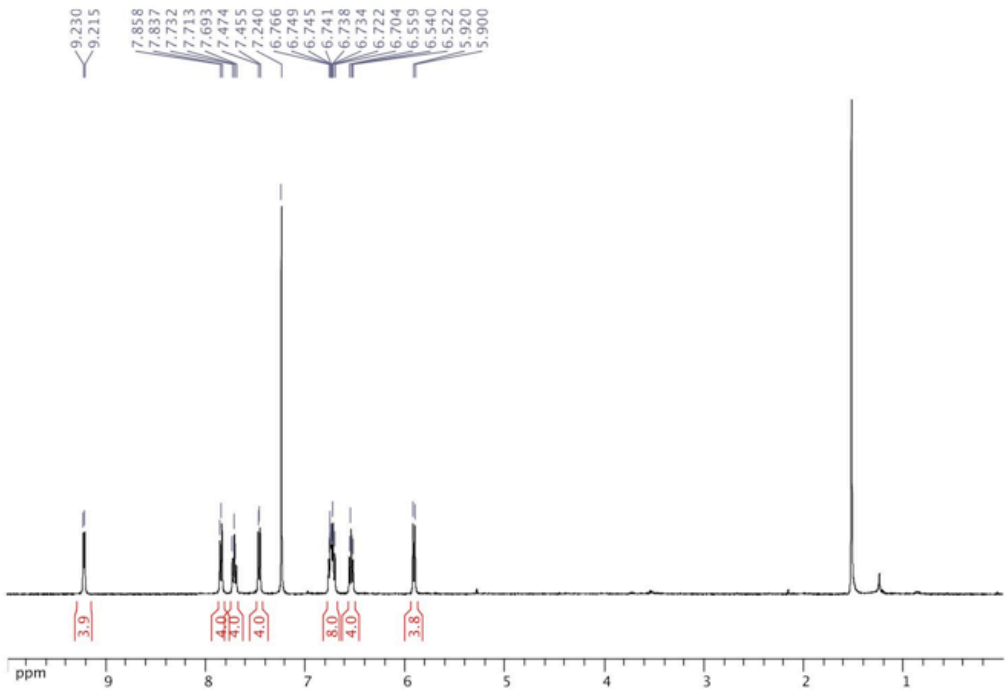

Figure S13. ^{1}H NMR of **[Ir(L1)$_2$(μ–Cl)]$_2$** in $CDCl_3$ (400 MHz, 25°C).

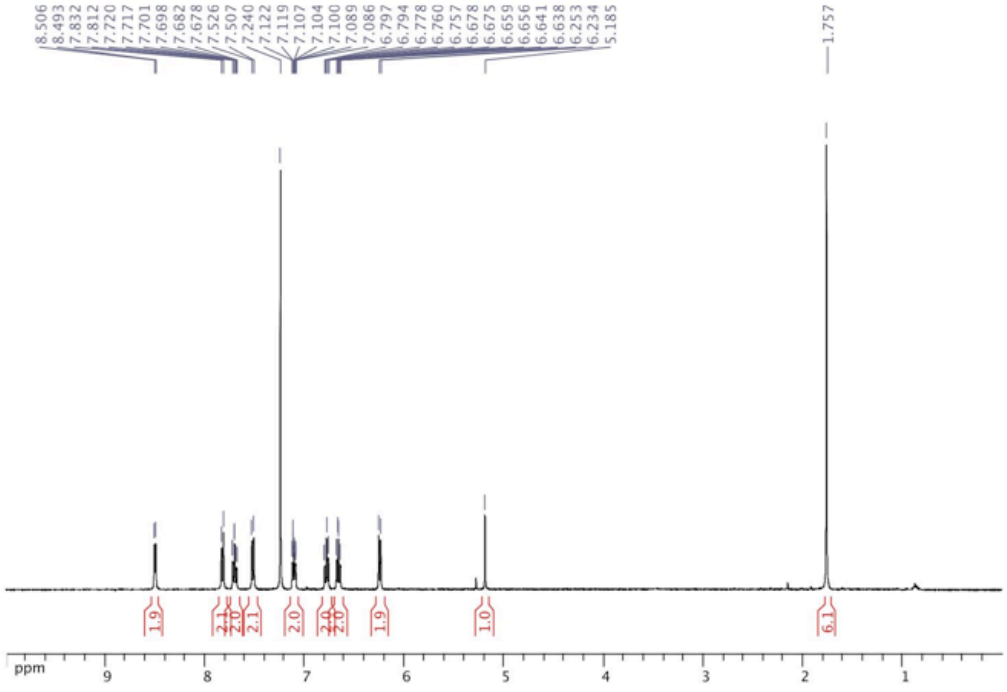

Figure S14. ^{1}H NMR of **1** in $CDCl_3$ (400 MHz, 25°C).

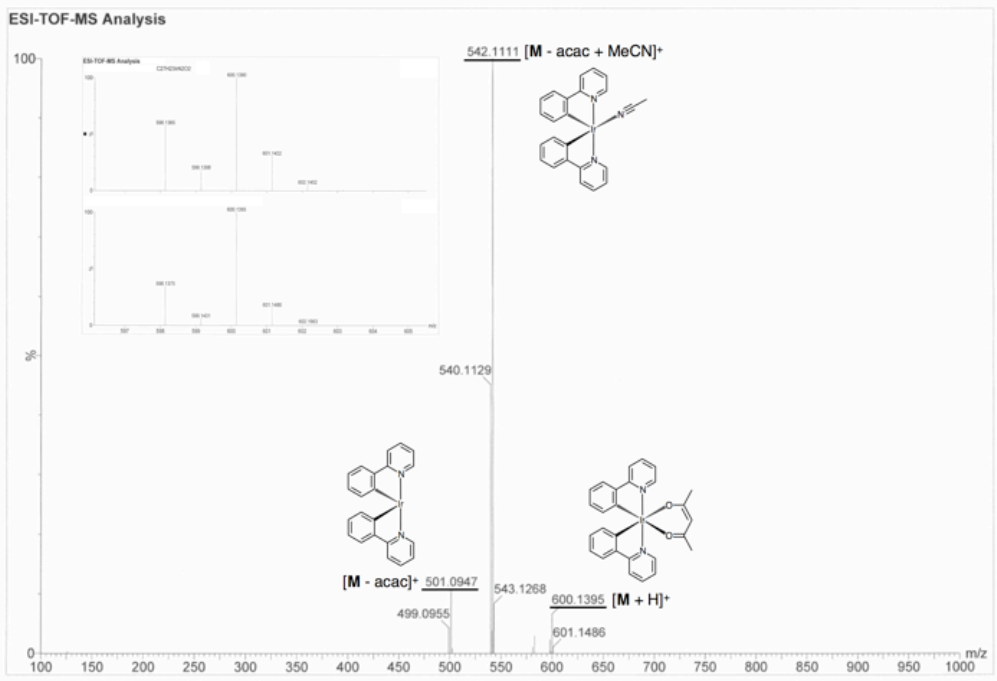

Figure S15. HR ES-MS of **1**.

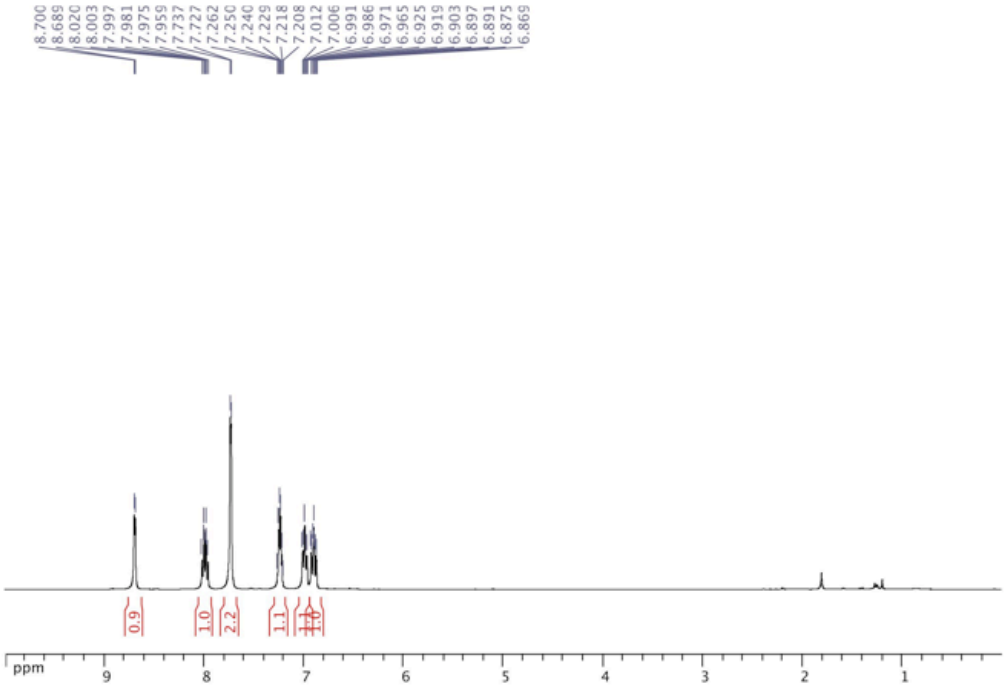

Figure S16. ^{1}H NMR of **L2** in $CDCl_3$ (400 MHz, 25°C).

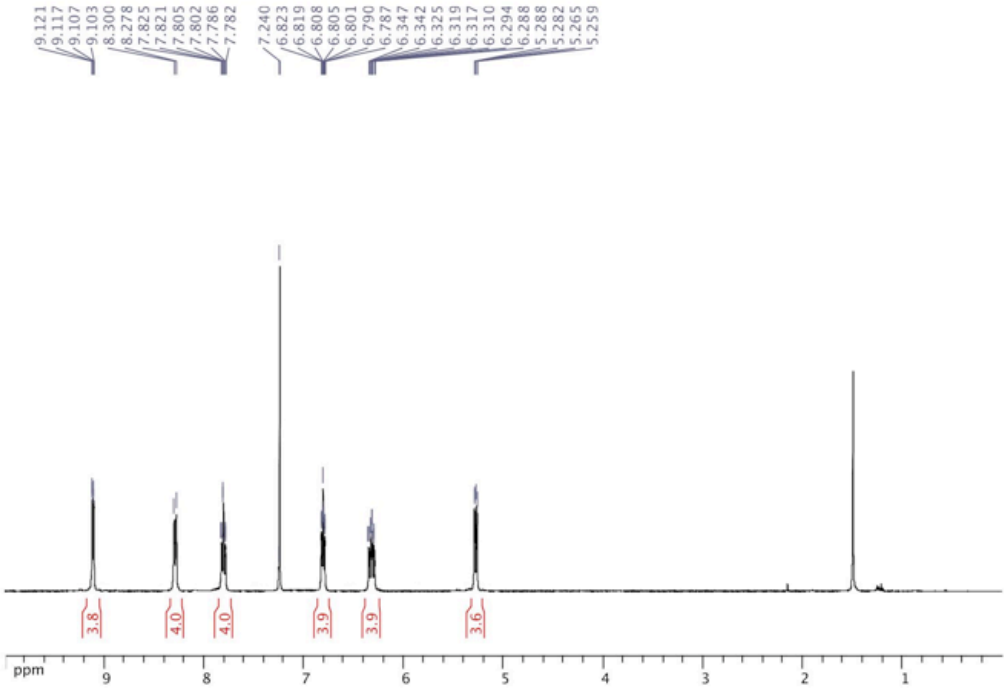

Figure S17. ^{1}H NMR of **[Ir(L2)$_2$(μ–Cl)]$_2$** in $CDCl_3$ (400 MHz, 25°C).

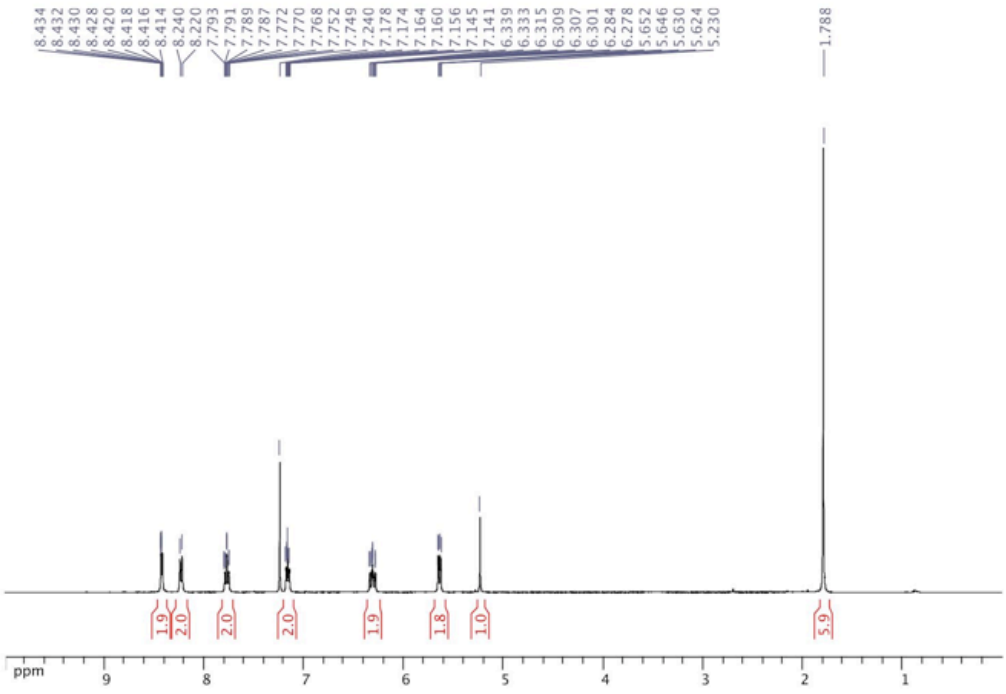

Figure S18. ^{1}H NMR of **2** in $CDCl_3$ (400 MHz, 25°C).

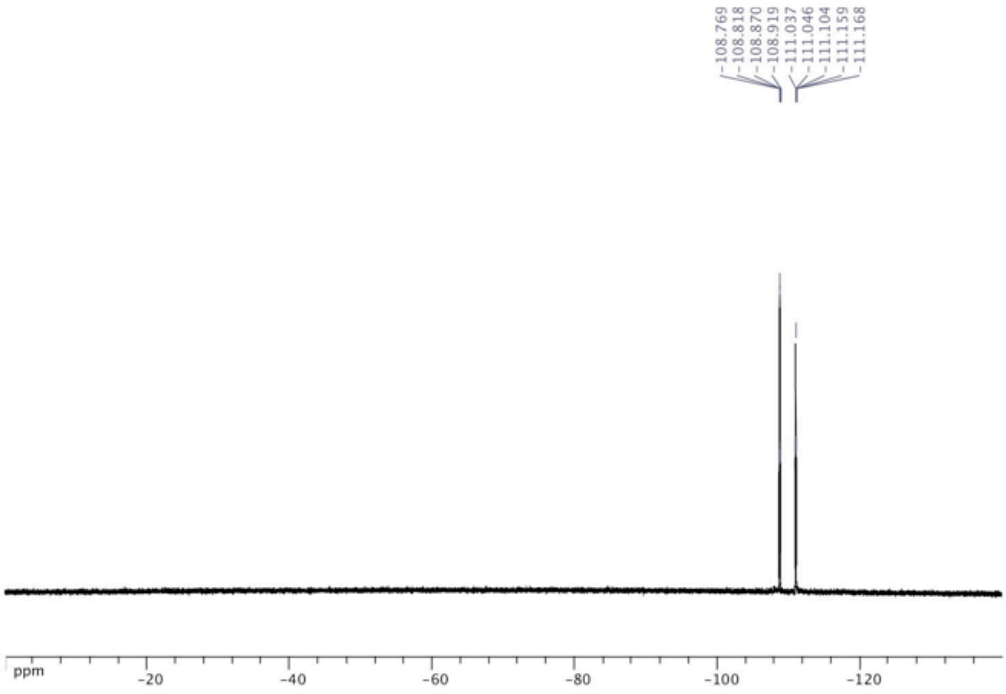

Figure S19. ^{19}F NMR of **2** in $CDCl_3$ (200 MHz, 25°C).

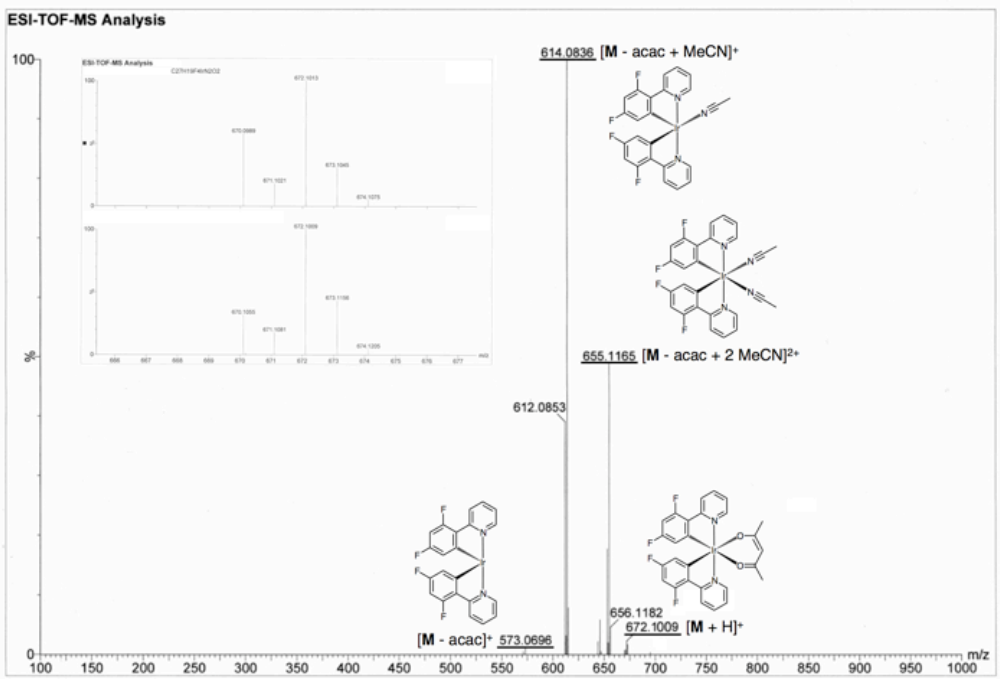

Figure S20. HR ES-MS of **2**.

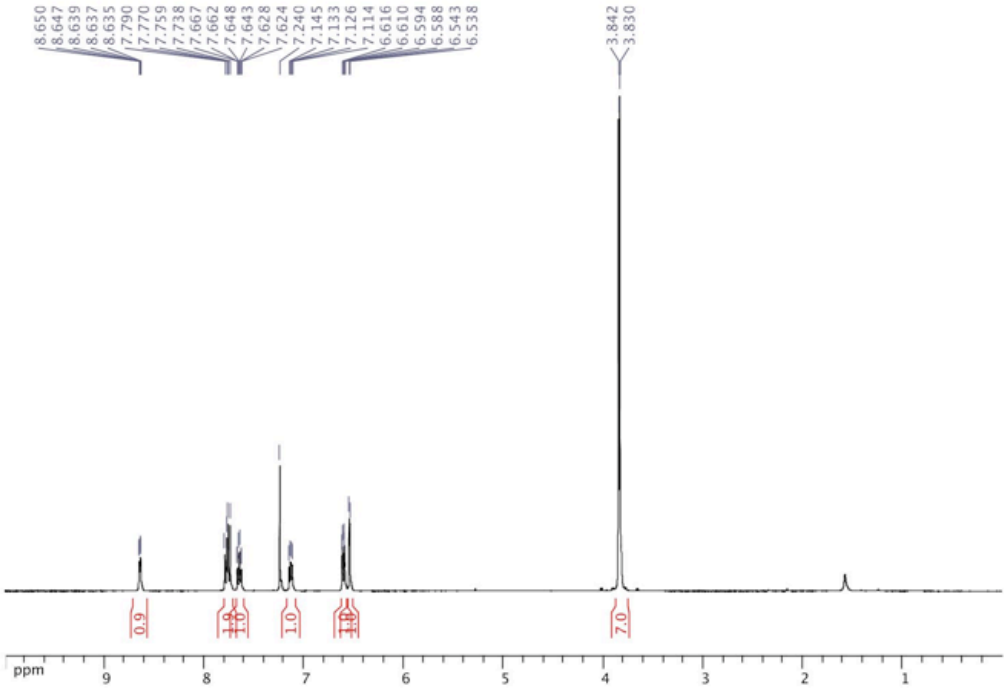

Figure S21. ^{1}H NMR of **L3** in $CDCl_3$ (400 MHz, 25°C).

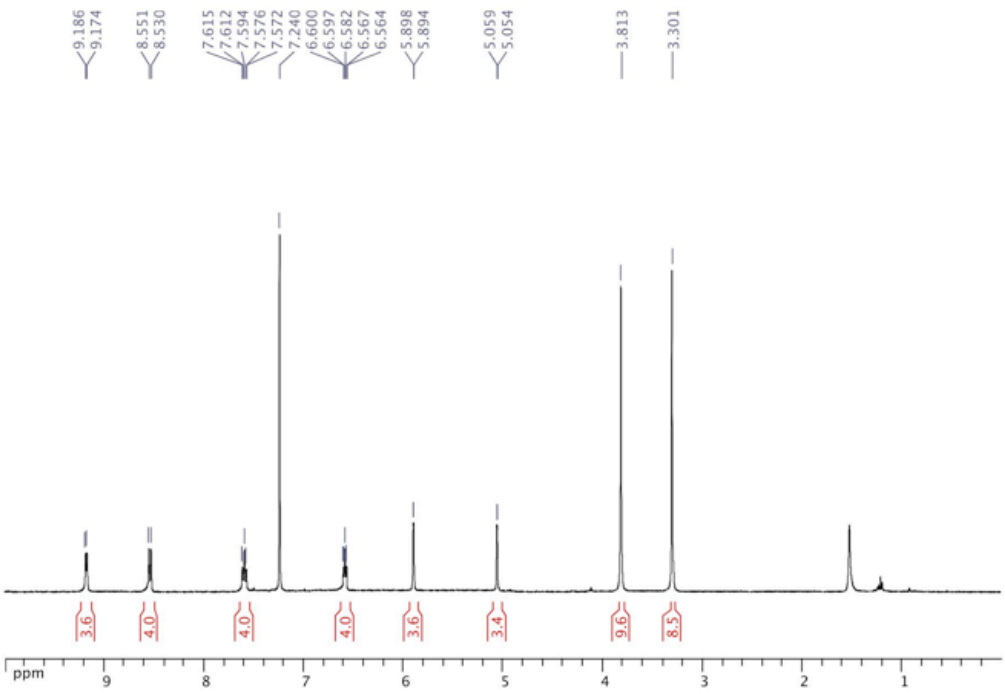

Figure S22. ^{1}H NMR of **[Ir(L3)$_2$(μ–Cl)]$_2$** in $CDCl_3$ (400 MHz, 25°C).

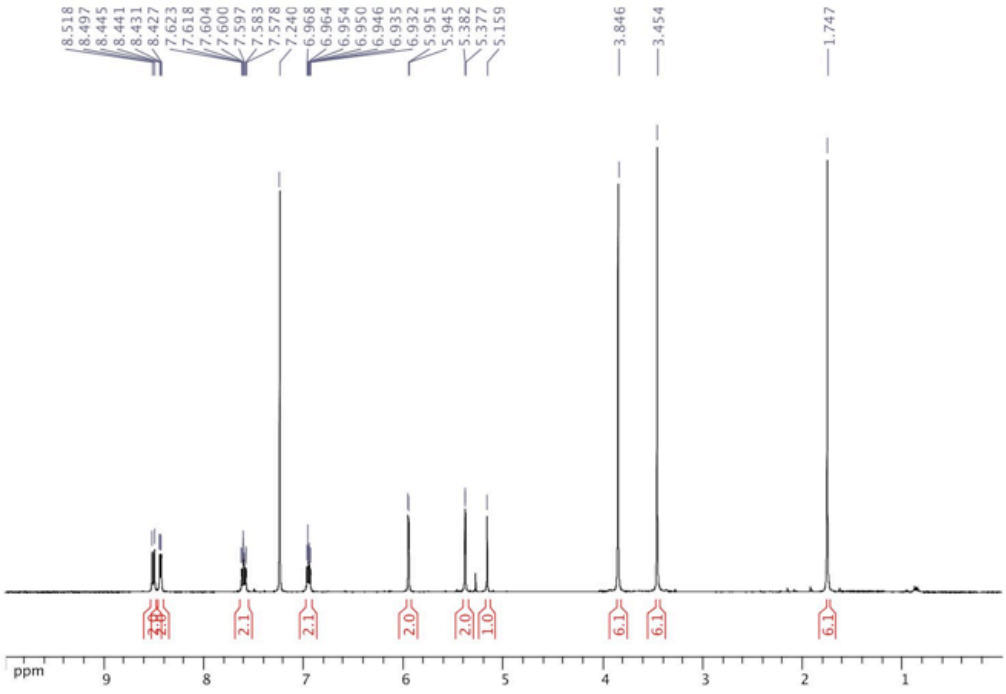

Figure S23. ^{1}H NMR of **3** in $CDCl_3$ (400 MHz, 25°C).

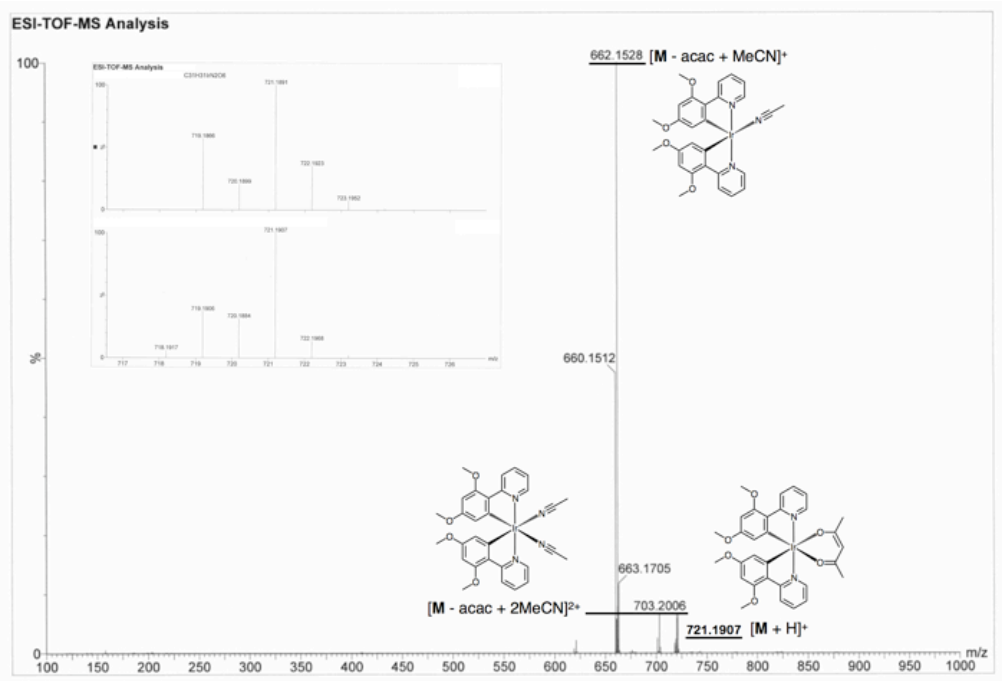

Figure S24. HR ES-MS of **3**.

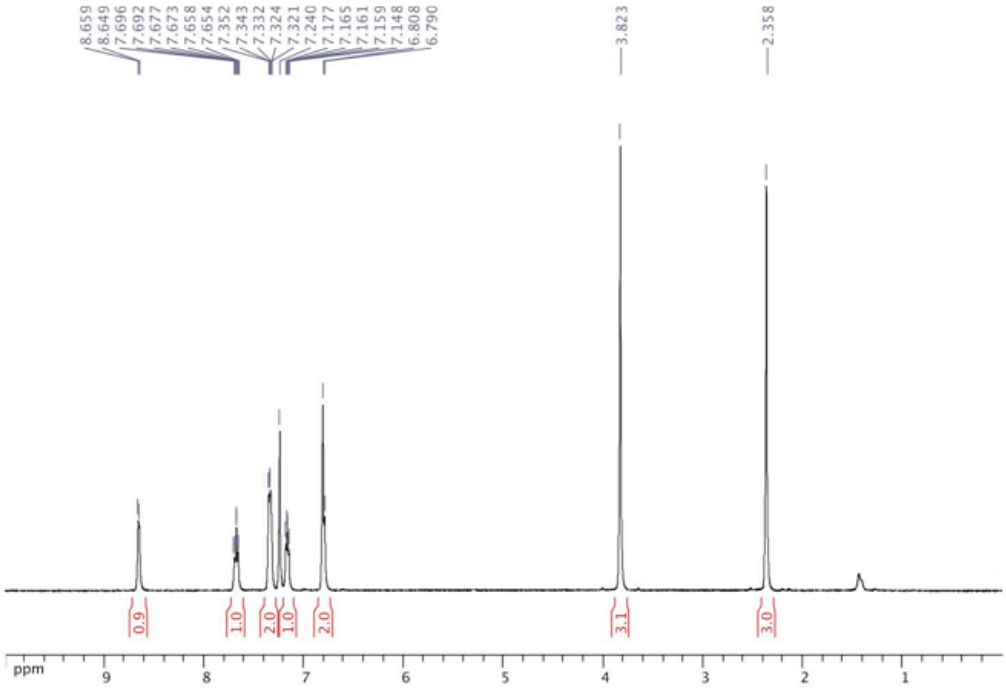

Figure S25. ^{1}H NMR of **L4** in $CDCl_3$ (400 MHz, 25°C).

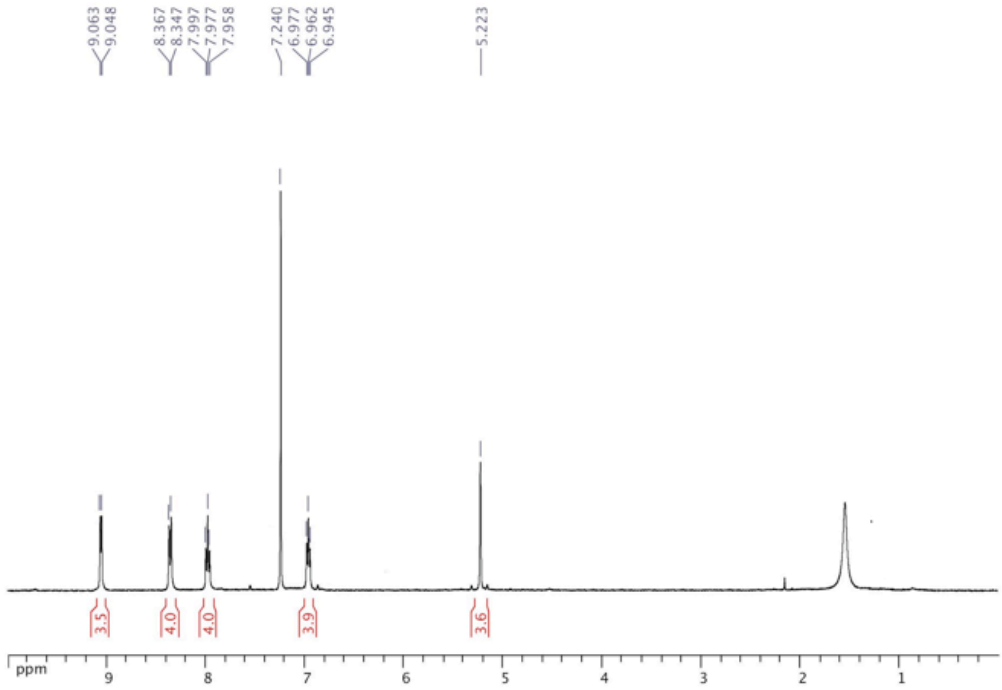

Figure S26. ^{1}H NMR of **[Ir(L4)$_2$(μ–Cl)]$_2$** in $CDCl_3$ (400 MHz, 25°C).

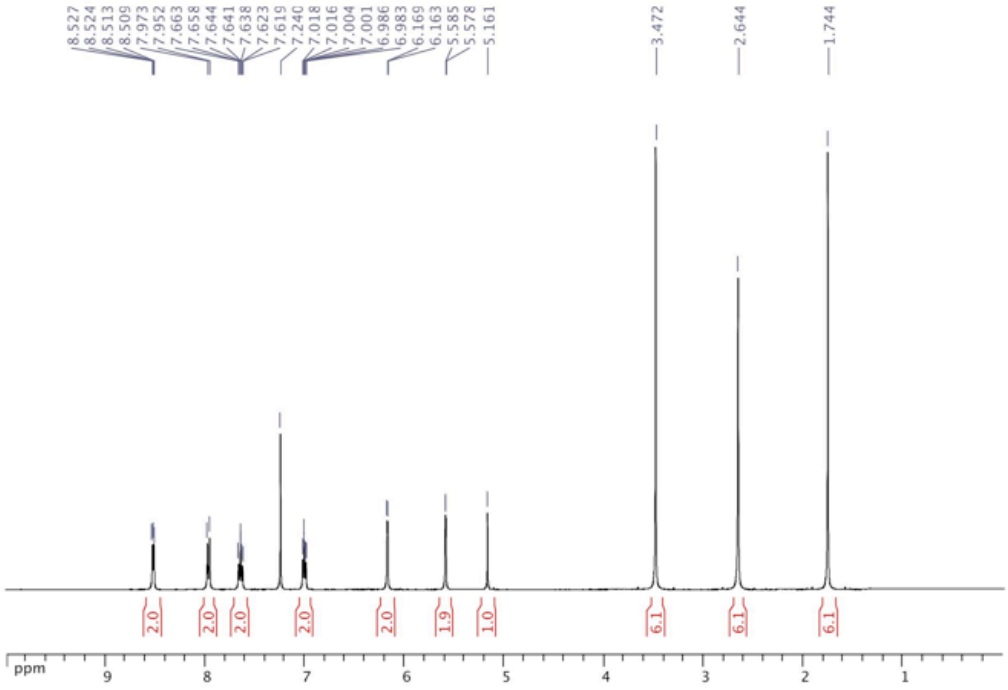

Figure S27. ^{1}H NMR of **4** in $CDCl_3$ (400 MHz, 25°C).

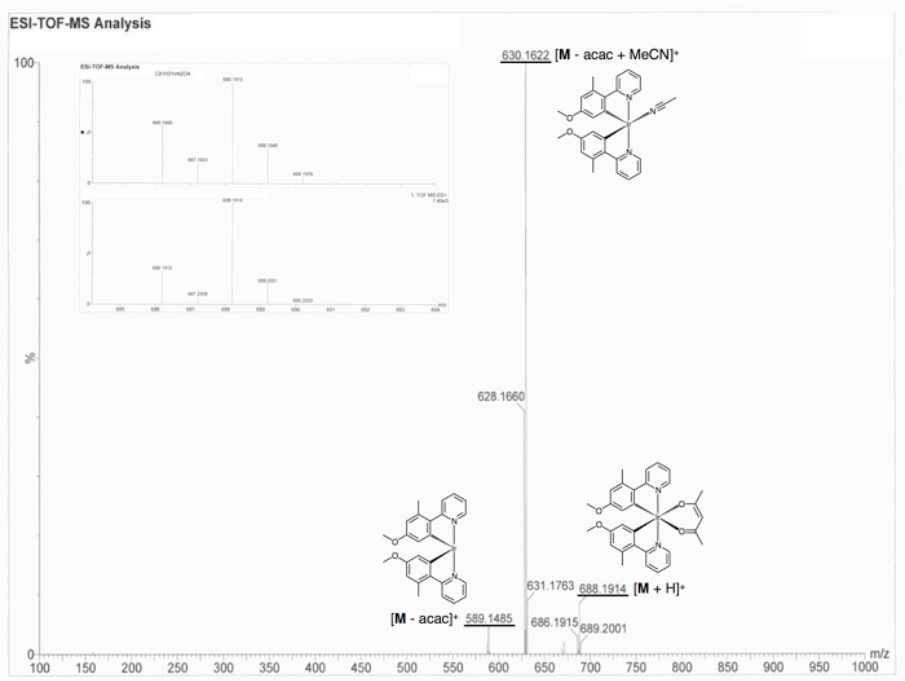

Figure S28. HR ES-MS of **4**.

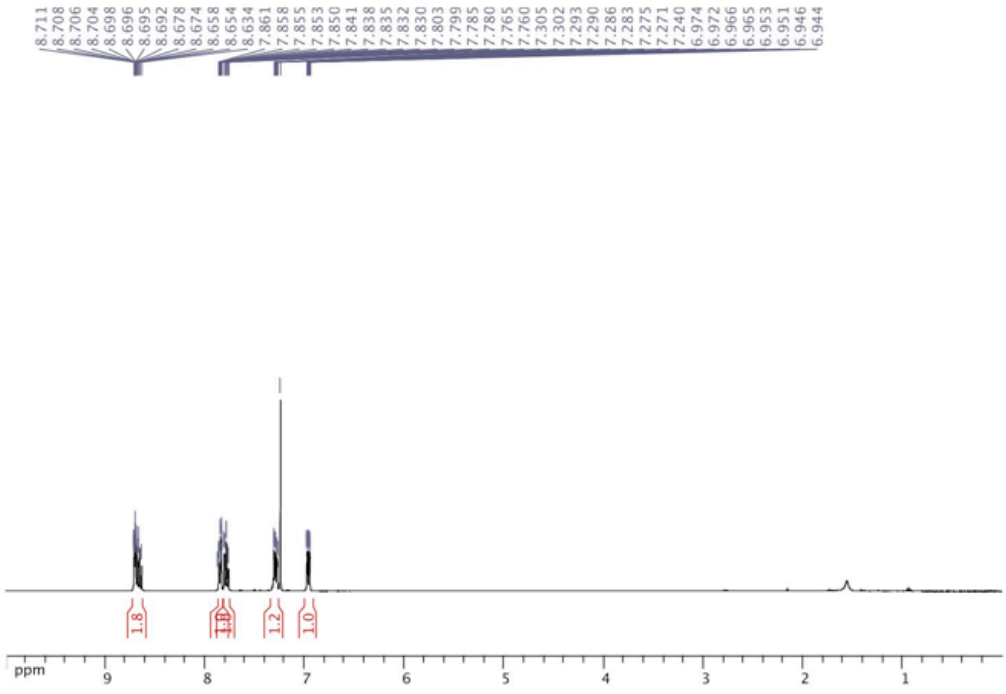

Figure S29. ^{1}H NMR of **L5** in $CDCl_3$ (400 MHz, 25°C).

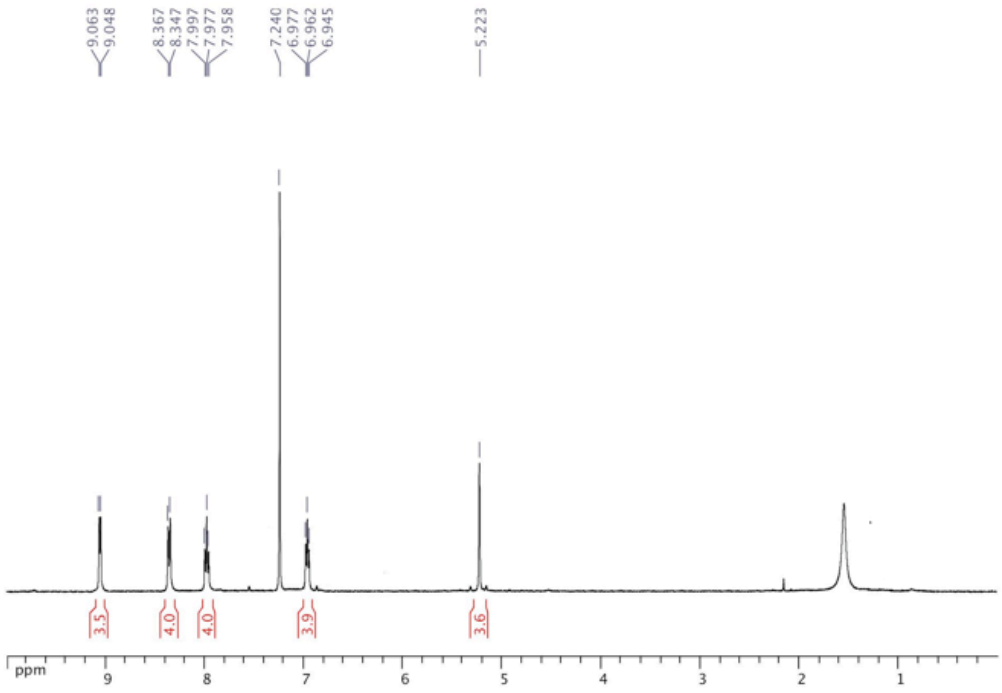

Figure S30. ^{1}H NMR of **[Ir(L5)$_2$(μ–Cl)]$_2$** in $CDCl_3$ (400 MHz, 25°C).

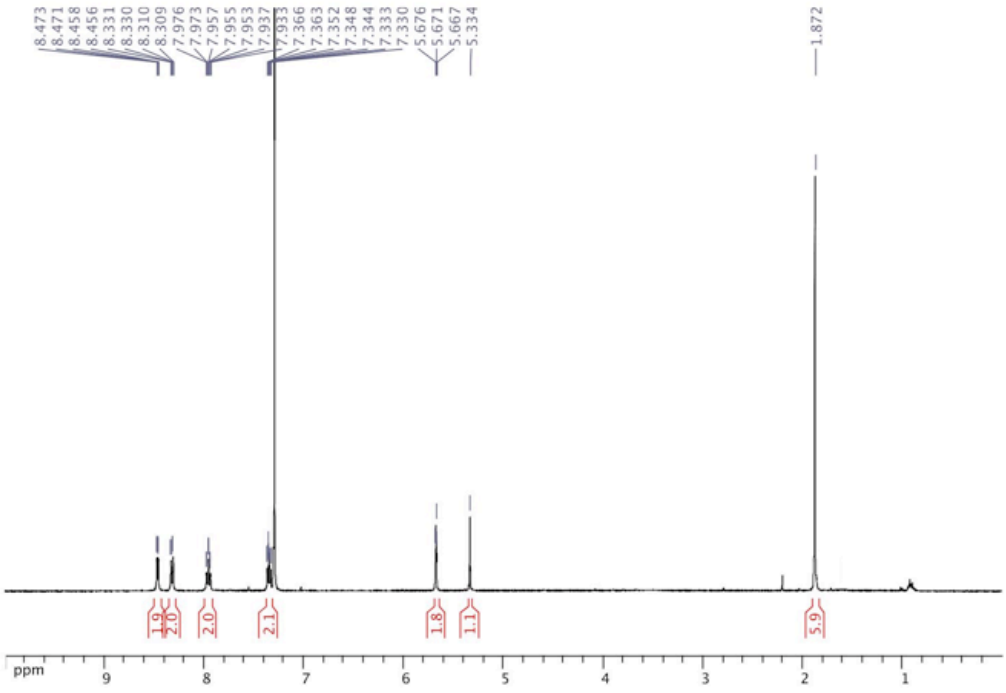

Figure S31. ^{1}H NMR of **5** in $CDCl_3$ (400 MHz, 25°C).

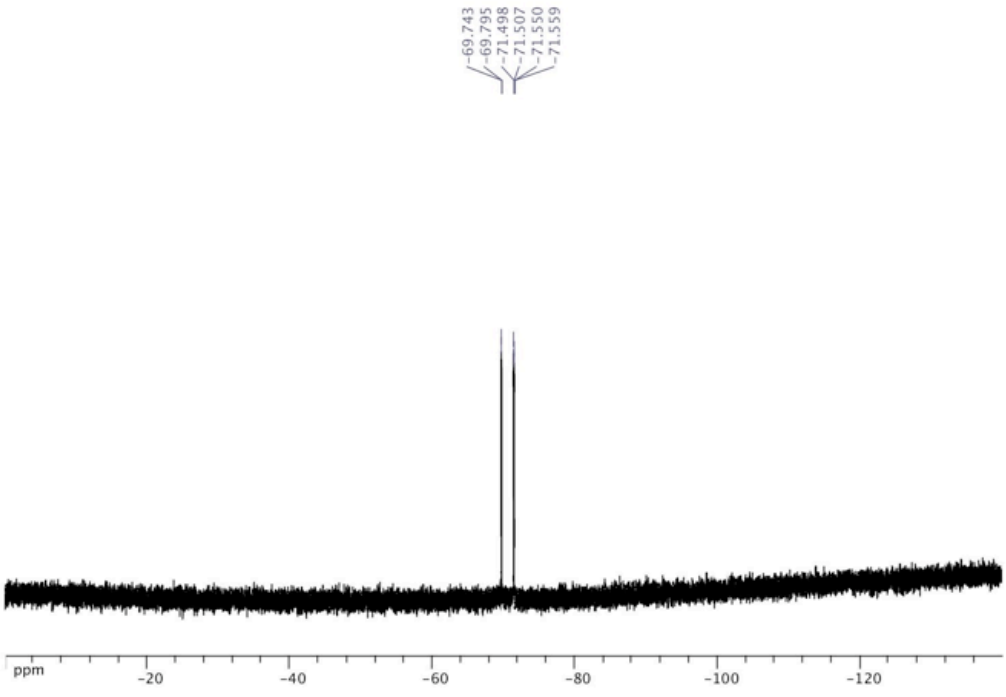

Figure S32. ^{19}F NMR of **5** in $CDCl_3$ (200 MHz, 25°C).

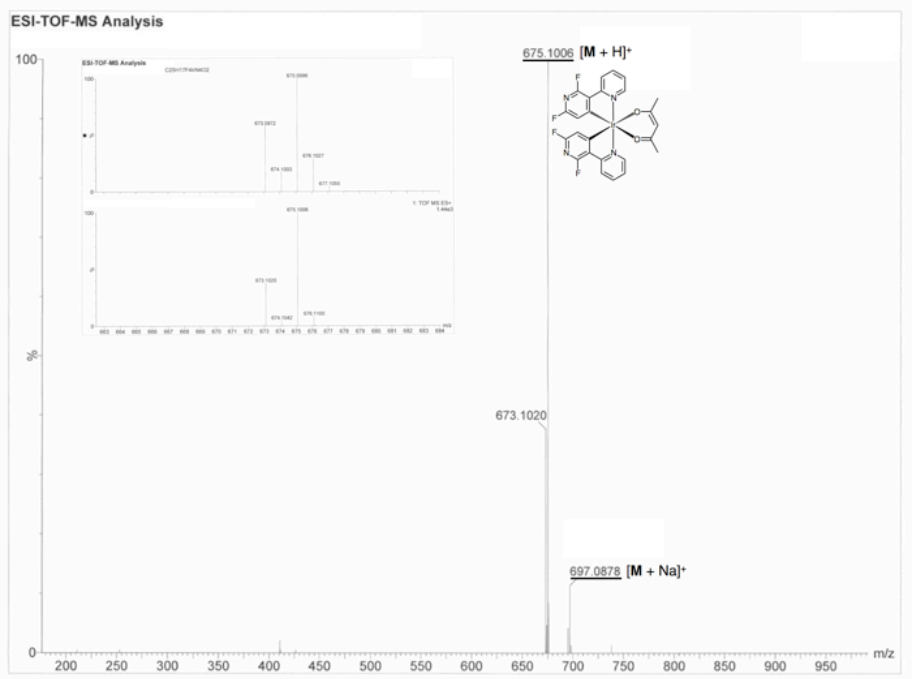

Figure S33. HR ES-MS of **5**.

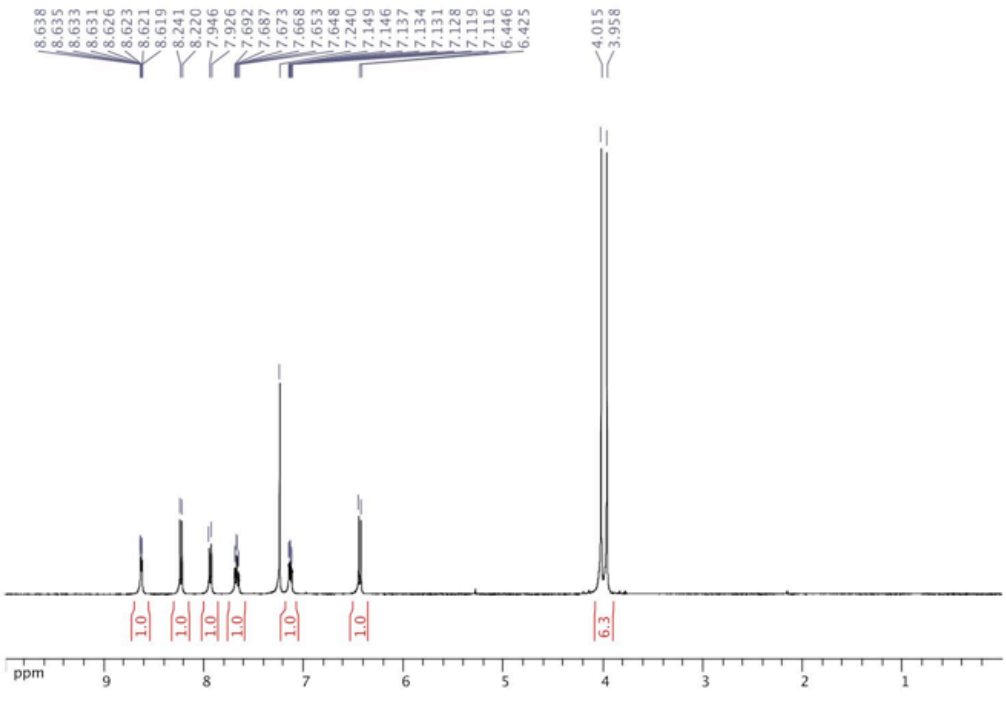

Figure S34. ^{1}H NMR of **L6** in $CDCl_3$ (400 MHz, 25°C).

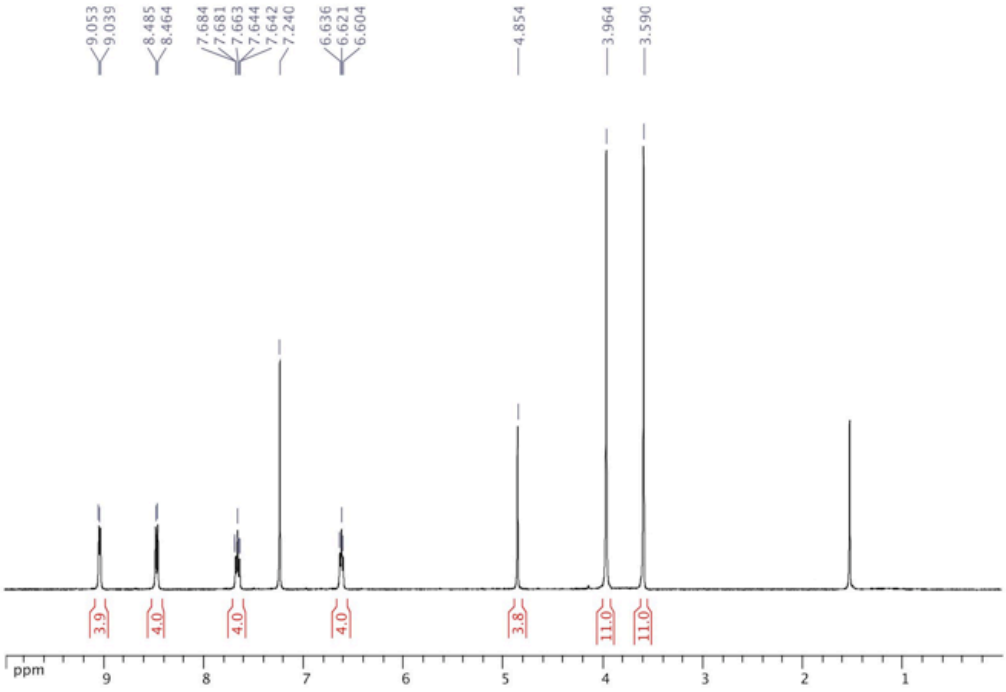

Figure S35. ^{1}H NMR of **[Ir(L6)$_2$(μ–Cl)]$_2$** in $CDCl_3$ (400 MHz, 25°C).

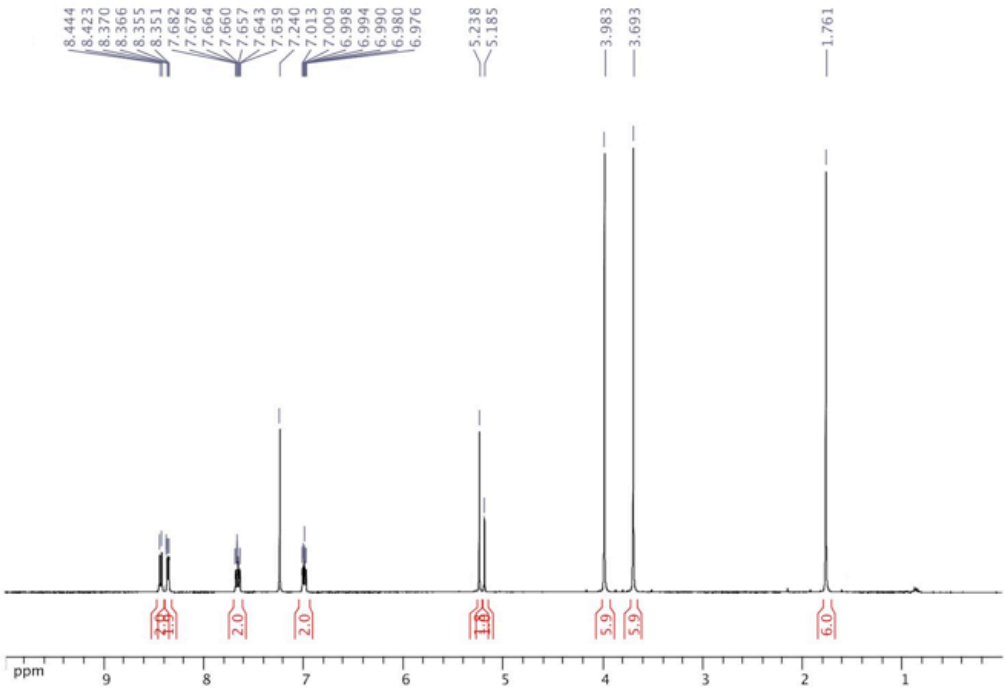

Figure S36. ^{1}H NMR of **6** in $CDCl_3$ (400 MHz, 25°C).

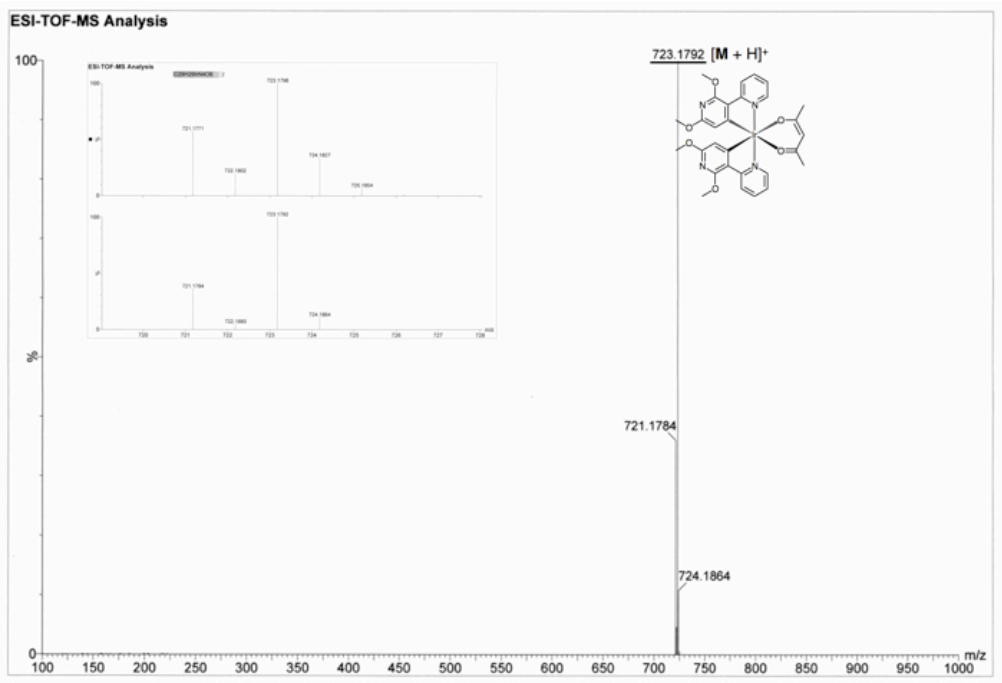

Figure S37. HR ES-MS of **6**.

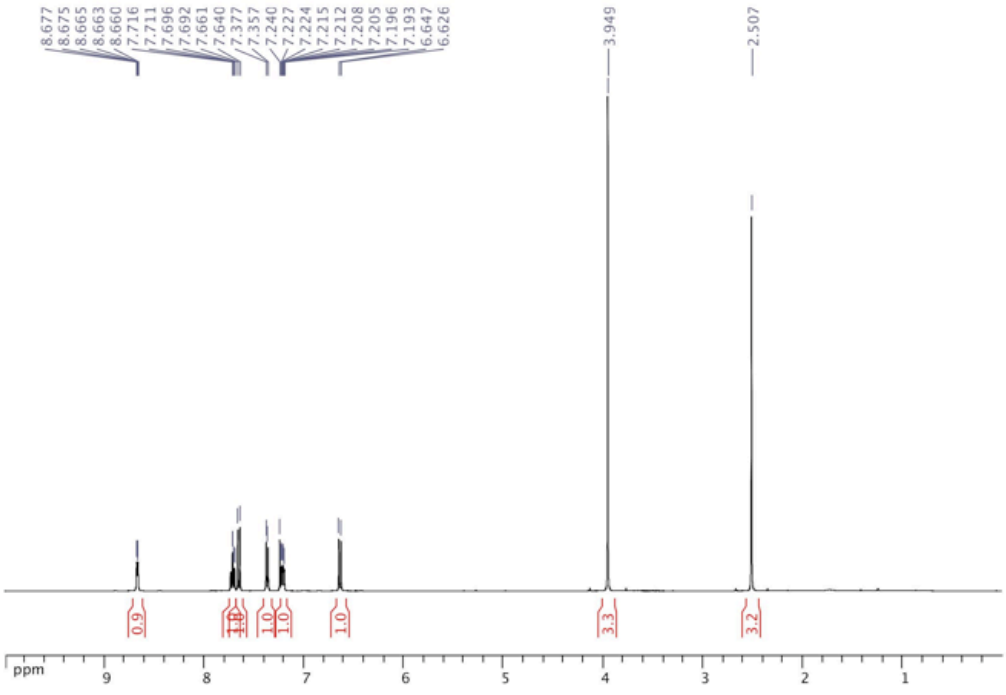

Figure S38. ^{1}H NMR of **L7** in $CDCl_3$ (400 MHz, 25°C).

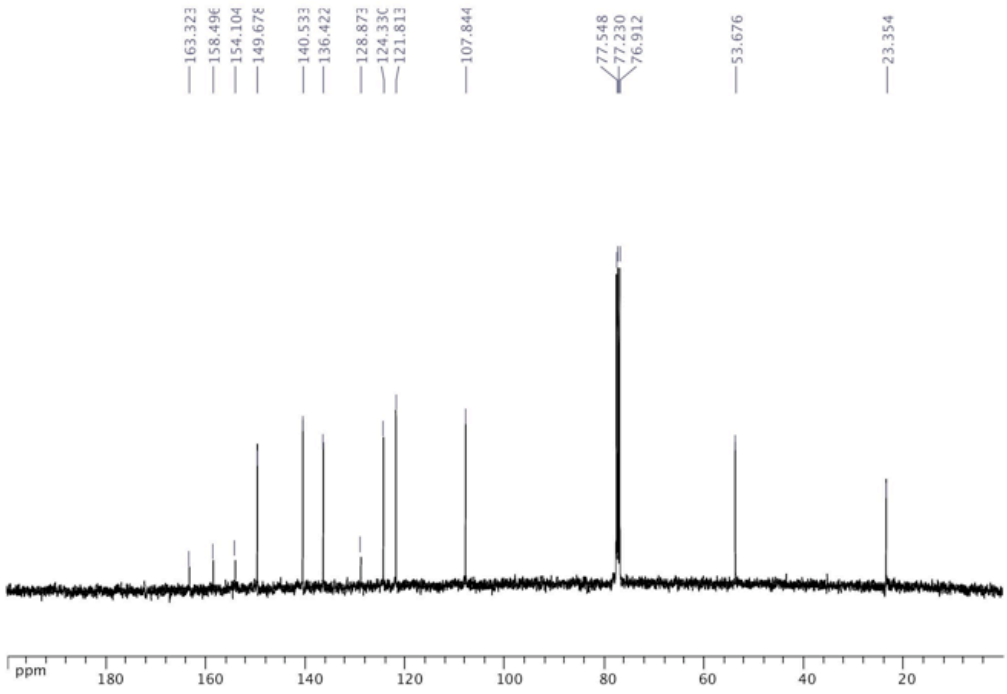

Figure S39. ^{13}C NMR of **L7** in $CDCl_3$ (100 MHz, 25°C).

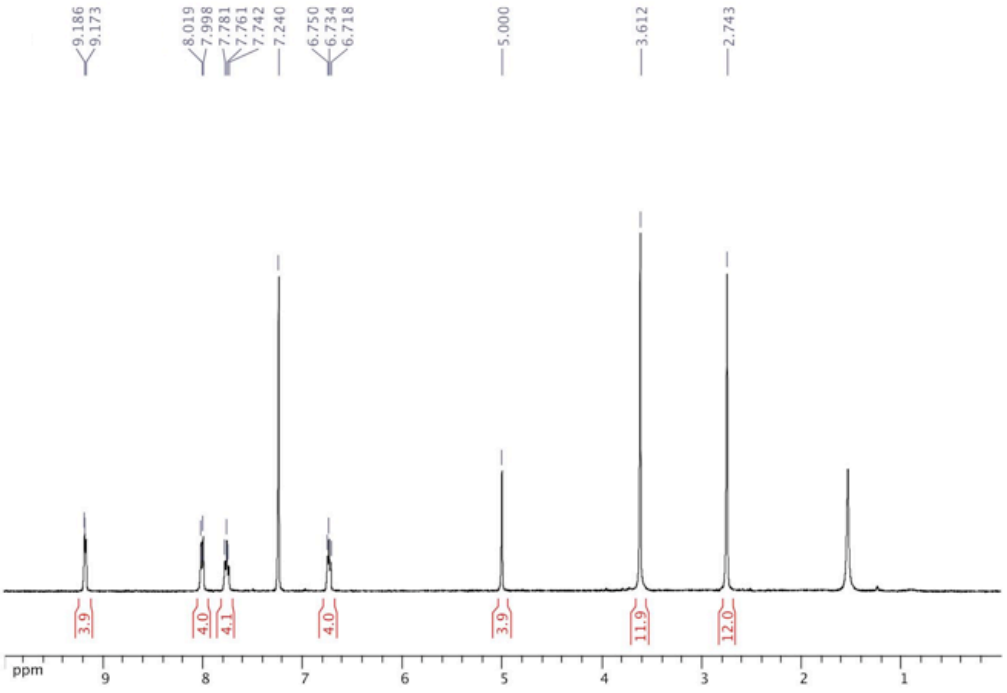

Figure S40. ^{1}H NMR of **[Ir(L7)$_2$(μ–Cl)]$_2$** in $CDCl_3$ (400 MHz, 25°C).

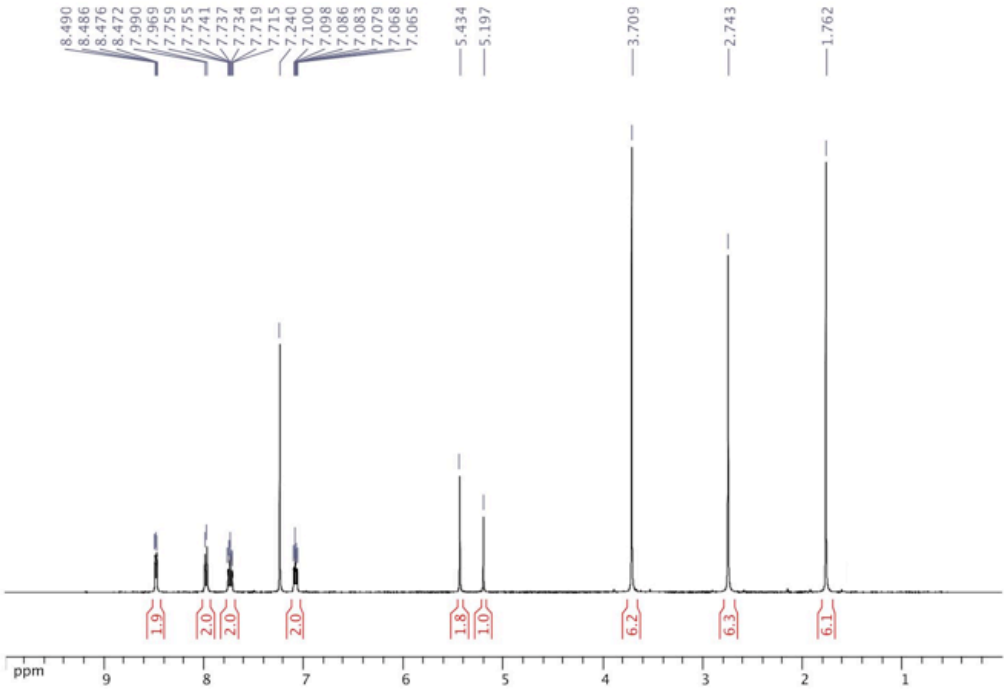

Figure S41. ^{1}H NMR of **7** in $CDCl_3$ (400 MHz, 25°C).

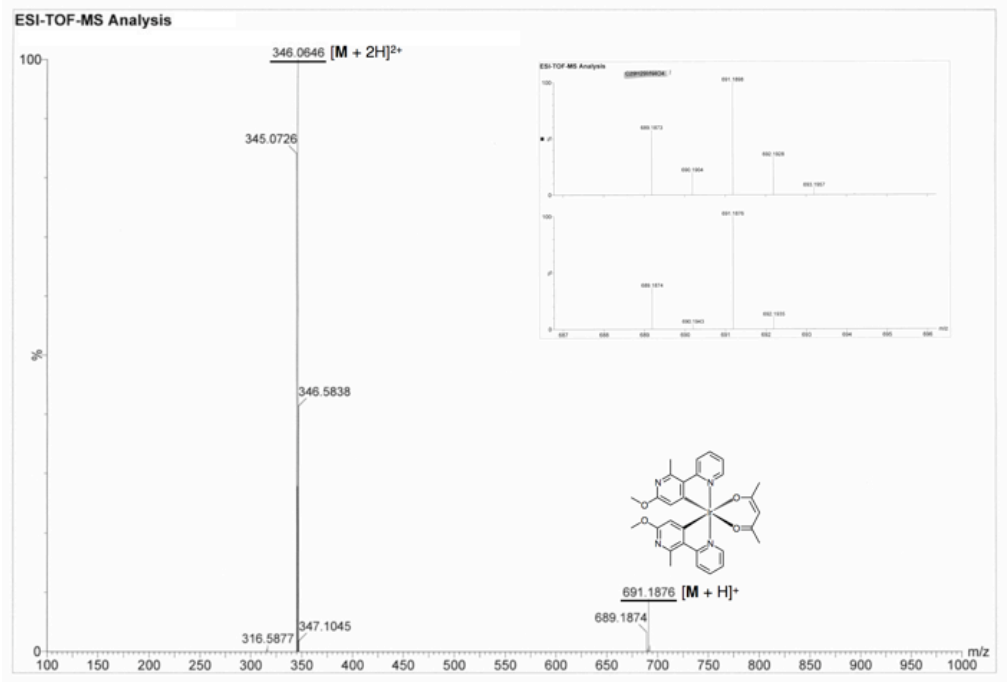

Figure S42. HR ES-MS of **7**.

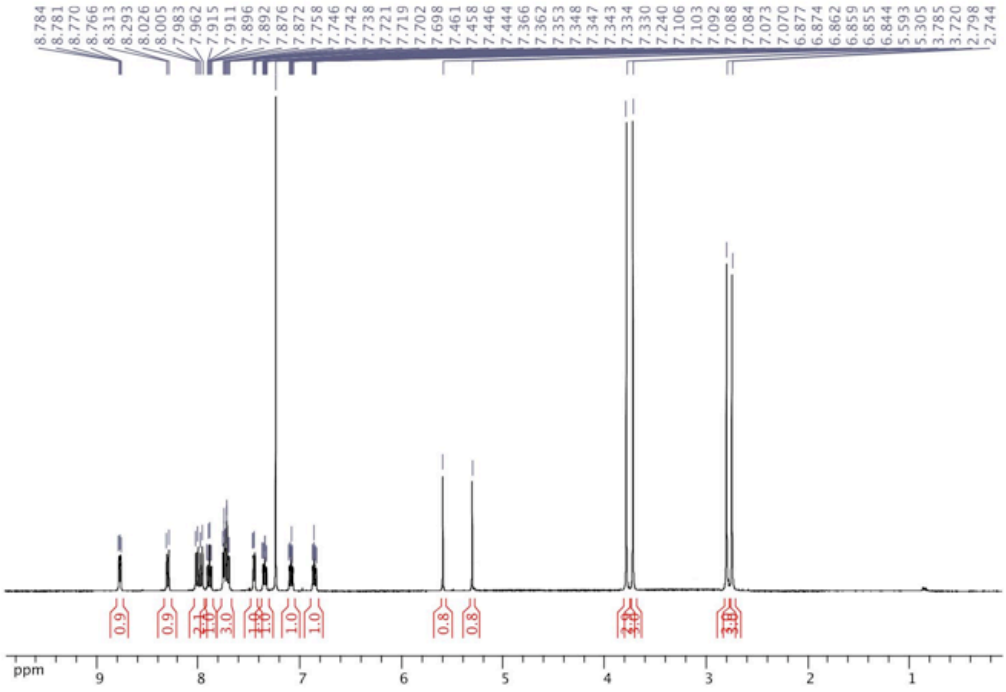

Figure S43. ^{1}H NMR of **EB343** in $CDCl_3$ (400 MHz, 25°C).

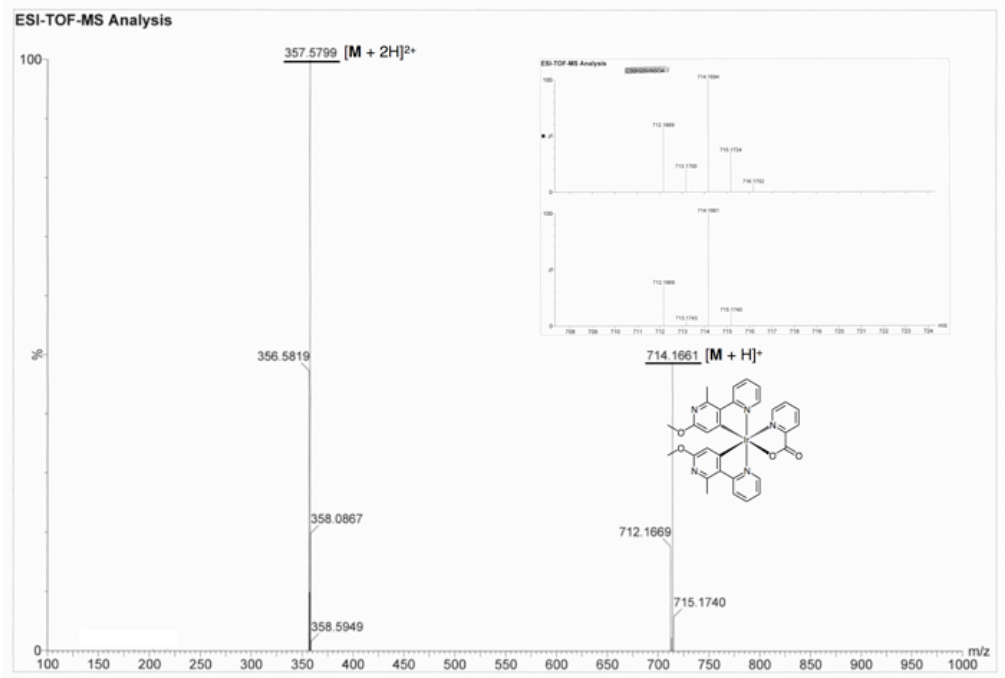

Figure S44. HR ES-MS of **EB343**.